

# Cross-correlations of the Lyman- $\alpha$ forest with weak lensing convergence I: Analytical Estimates of S/N and Implications for Neutrino Mass and Dark Energy

Alberto Vallinotto\*

*Center for Particle Astrophysics, Fermi National Accelerator Laboratory,  
P.O. Box 500, Kirk Rd. & Pine St., Batavia, IL 60510-0500 USA*

Matteo Viel†

*INAF - Osservatorio Astronomico di Trieste, Via G.B. Tiepolo 11, I-34131 Trieste, Italy  
INFN - National Institute for Nuclear Physics, Via Valerio 2, I-34127 Trieste, Italy*

Sudeep Das‡

*Princeton University Observatory, Peyton Hall, Ivy Lane, Princeton, NJ 08544 USA  
Berkeley Center for Cosmological Physics, LBNL and Department of Physics, University of California, Berkeley, CA 94720.*

David N. Spergel§

*Princeton University Observatory, Peyton Hall, Ivy Lane, Princeton, NJ 08544 USA*

(Dated: October 22, 2009)

We expect a detectable correlation between two seemingly unrelated quantities: the four point function of the cosmic microwave background (CMB) and the amplitude of flux decrements in quasar (QSO) spectra. The amplitude of CMB convergence in a given direction measures the projected surface density of matter. Measurements of QSO flux decrements trace the small-scale distribution of gas along a given line-of-sight. While the cross-correlation between these two measurements is small for a single line-of-sight, upcoming large surveys should enable its detection. This paper presents analytical estimates for the signal to noise (S/N) for measurements of the cross-correlation between the flux decrement and the convergence,  $\langle \delta\mathcal{F}\kappa \rangle$ , and for measurements of the cross-correlation between the variance in flux decrement and the convergence,  $\langle (\delta\mathcal{F})^2 \kappa \rangle$ . For the ongoing BOSS (SDSS III) and Planck surveys, we estimate an S/N of 30 and 9.6 for these two correlations. For the proposed BigBOSS and ACTPOL surveys, we estimate an S/N of 130 and 50 respectively. Since  $\langle (\delta\mathcal{F})^2 \kappa \rangle \propto \sigma_8^4$ , the amplitude of these cross-correlations can potentially be used to measure the amplitude of  $\sigma_8$  at  $z \sim 2$  to 2.5% with BOSS and Planck and even better with future data sets. These measurements have the potential to test alternative theories for dark energy and to constrain the mass of the neutrino. The large potential signal estimated in our analytical calculations motivate tests with non-linear hydrodynamical simulations and analyses of upcoming data sets.

PACS numbers: 98.62.Ra, 98.70.Vc, 95.30.Sf

## I. INTRODUCTION

The confluence of high resolution Cosmic Microwave Background (CMB) experiments and large-scale spectroscopic surveys in the near future is expected to sharpen our view of the Universe. Arcminute scale CMB experiments such as Planck [1], the Atacama Cosmology Telescope [2, 3], the South Pole Telescope [4, 5], QUIET [6] and PolarBear [7], will chart out the small scale anisotropies in the CMB. This will shed new light on the primordial physics of inflation, as well as the astrophysics of the low redshift Universe through the signatures of the interactions of the CMB photons with large scale structure. Spectroscopic surveys like BOSS [8, 9] and BigBOSS [10] will trace the large scale structure of neutral

gas, probing the distribution and dynamics of matter in the Universe. While these two datasets will be rich on their own, they will also complement and constrain each other. An interesting avenue for using the two datasets would be to utilize the fact that the arcminute-scale secondary anisotropies in the CMB are signatures of the same large scale structure that is traced by the spectroscopic surveys, and study them in cross-correlation with each other. In this paper, we present the analytic estimates for one such cross correlation candidate - that between the gravitational lensing of the CMB and the flux fluctuations in the Lyman- $\alpha$  forest.

The gravitational lensing of the CMB, or CMB lensing in short, is caused by the deflection of the CMB photons by the large scale structure potentials [see 11, for a review]. On large scales, WMAP measurements imply that the primordial CMB is well described as an isotropic Gaussian random field [12]. On small scales, lensing breaks this isotropy and introduces a specific form of non-Gaussianity. These properties of the lensed CMB sky can be used to construct estimators of the deflection field that lensed the CMB. Therefore, CMB lensing pro-

---

\*Electronic address: avalli@fnal.gov

†Electronic address: viel@oats.inaf.it

‡Electronic address: sudeep@astro.princeton.edu

§Electronic address: dns@astro.princeton.edu

vides us with a way of reconstructing a line-of-sight (los) projected density field from zero redshift to the last scattering surface, with a broad geometrical weighting kernel that gets most of its contribution from the  $z = 1 - 4$  range [13–15]. While CMB lensing is mainly sensitive to the geometry and large scale projected density fluctuations, the Lyman- $\alpha$  forest, the absorption in quasar (QSO) spectra caused by intervening neutral hydrogen in the intergalactic medium, primarily traces the small-scale distribution of gas (and hence, also matter) along the line of sight.

A cross-correlation between these two effects gives us a unique way to study how small scale fluctuations in the density field evolve on top of large scale over and under-densities, and how gas traces the underlying dark matter. This signal is therefore a useful tool to test to what extent the fluctuations in the Lyman- $\alpha$  flux relate to the underlying dark matter. Once that relationship is understood, it can also become a powerful probe of the growth of structure on a wide range of scales. Since both massive neutrinos and dark energy alter the growth rate of structure at  $z \sim 2$ , these measurements can probe their effects. This new cross-correlation signal, should also be compared with other existing cross-correlations between CMB and LSS that have already been observed and that are sensitive to different redshift regimes [16–20].

In this work, we build an analytic framework based on simplifying assumptions to estimate the cross-correlation of the first two moments of the Lyman- $\alpha$  flux fluctuation with the weak lensing convergence  $\kappa$ , obtained from CMB lensing reconstruction, measured along the same line of sight. The finite resolution of the spectrogram limits the range of parallel  $k$ -modes probed by the absorption spectra and the finite resolution of the CMB experiments limits the range of perpendicular  $k$ -modes probed by the convergence measurements. These two effect break the spherical symmetry of the  $k$ -space integration. However, we show that by resorting to a power series expansion it is still possible to obtain computationally efficient expressions for the evaluation of the signal.

We then investigate the detectability of the signal in upcoming CMB and LSS surveys, and the extent to which such a signal can be used as a probe of neutrino masses and early dark energy scenarios. A highlight of our results is that the estimated cross-correlation signal seems to have significant sensitivity to the normalization of the matter power spectrum  $\sigma_8$ . Consistency with CMB measurements – linking power spectrum normalization and the sum of the neutrino masses – allows to use this cross-correlation to put additional constrain on the latter.

The structure of the paper is as follows. In Section II we introduce the two physical observables, the Lyman- $\alpha$  flux and the CMB convergence (II A), the cross-correlation estimators (II B) and their variances (II C). Our main result is presented in section II D where the signal-to-noise ratios are computed. Section II E contains a spectral analysis of the observables that aims at finding the Lyman- $\alpha$  wavenumbers that contribute most to such

a signal. We focus on two cosmologically relevant applications in sections III A and III B, for massive neutrinos and early dark energy models, respectively. We conclude with a discussion in section IV.

## II. ANALYTICAL RESULTS

### A. Physical Observables

#### *Fluctuations in the Lyman- $\alpha$ flux*

Using the *fluctuating Gunn–Peterson approximation* [21], the transmitted flux  $\mathcal{F}$  along a los  $\hat{n}$  is related to the density fluctuations of the intergalactic medium (IGM)  $\delta_{\text{IGM}}$  by

$$\mathcal{F}(\hat{n}, z) = \exp \left[ -A (1 + \delta_{\text{IGM}}(\hat{n}, z))^{\beta} \right], \quad (1)$$

where  $A$  and  $\beta$  are two functions relating the flux fluctuation to the dark matter overdensities. These two functions depend on the redshift considered:  $A$  is of order unity and is related to the mean flux level, baryon fraction, IGM temperature, cosmological parameters and the photoionization rate of hydrogen. A good approximation for its redshift dependence is  $A(z) \approx 0.0023 (1 + z)^{3.65}$  (see [22]).  $\beta$  on the other hand depends on to the so-called IGM temperature-density relation and in particular on the power-law index of this relation (e.g. [23, 24]) and should be less dependent on redshift (unless temperature fluctuations due for example to reionization play a role, see [25]). For the calculation of signal/noise in the paper, we neglect the evolution of  $A$  and  $\beta$  with redshift. While the value of the correlators considered will depend on  $A$  and  $\beta$ , their signal-to-noise (S/N) ratio will not.

On scales larger than about  $1 h^{-1} \text{Mpc}$  (comoving), which is about the Jeans length at  $z = 3$ , the relative *fluctuations* in the Lyman- $\alpha$  flux  $\delta\mathcal{F} \equiv (\mathcal{F} - \bar{\mathcal{F}})/\bar{\mathcal{F}}$  are proportional to the fluctuations in the IGM density field [26–30]. We assume that the IGM traces the dark matter on large scales,

$$\delta\mathcal{F}(\hat{n}, \chi) \approx -A\beta\delta_{\text{IGM}}(\hat{n}, \chi) \approx -A\beta\delta(\hat{n}, \chi). \quad (2)$$

The (variance of the) flux fluctuation in the redshift range covered by the Lyman- $\alpha$  spectrum is then proportional to (the variance of) the fluctuations in dark matter

$$\begin{aligned} \delta\mathcal{F}^r(\hat{n}) &= \int_{\chi_i}^{\chi_Q} d\chi \delta\mathcal{F}^r(\hat{n}, \chi) \\ &\approx \int_{\chi_i}^{\chi_Q} d\chi (-A\beta)^r \delta^r(\hat{n}, \chi), \end{aligned} \quad (3)$$

where the range of comoving distances probed by the Lyman- $\alpha$  spectrum extends from  $\chi_i$  to  $\chi_Q$ . The  $r = 1$  case corresponds to the fluctuations in the flux and the  $r = 2$  case corresponds to their variance. We stress that the above approximation is valid in linear theory

neglecting not only the non-linearities produced by gravitational collapse but also those introduced by the definition of the flux and those produced by the thermal broadening and peculiar velocities. Note that while the assumption of “tracing” between gas and dark matter distribution above the Jeans length is expected in the standard linear perturbation theory [31], the one between the flux and the matter has been verified a-posteriori using semi-analytical methods ([26, 32]) and numerical simulations ([27, 33, 34]) that successfully reproduce most of the observed Lyman- $\alpha$  properties. Furthermore, non-gravitational processes such as temperature and/or ultra-violet fluctuations in the IGM should alter the Lyman- $\alpha$  forest flux power and correlations in a distinct way as compared to the gravitational instability process and to linear evolution (e.g. [35–37]).

### *Cosmic Microwave Background convergence field*

The effective weak lensing convergence  $\kappa(\hat{n})$  measured along a los in the direction  $\hat{n}$  is proportional to the dark matter overdensity  $\delta$  through

$$\kappa(\hat{n}, \chi_F) = \frac{3H_0^2\Omega_m}{2c^2} \int_0^{\chi_F} d\chi W_L(\chi, \chi_F) \frac{\delta(\hat{n}, \chi)}{a(\chi)}, \quad (4)$$

where the integral along the los extends up to a comoving distance  $\chi_F$  and where  $W_L(\chi, \chi_F) = \chi(\chi_F - \chi)/\chi_F$  is the lensing window function. In what follows we consider the cross-correlation of Lyman- $\alpha$  spectra with the convergence field measured from the CMB, as in Vallinotto et al. [38], in which case  $\chi_F$  is the comoving distance to the last scattering surface. Note however that it is straightforward to extend the present treatment to consider the cross-correlation of the Lyman- $\alpha$  flux fluctuations with convergence maps constructed from other data sets, like optical galaxy surveys.

It is necessary to stress here that Eq. (1) above depends on the density fluctuations in the IGM, which in principle are distinct from the ones in the dark matter, whereas  $\kappa$  depends on the dark matter overdensities  $\delta$ . If the IGM and dark matter overdensity fields were completely independent, the cross-correlation between them would inevitably yield zero. If however the fluctuations in the IGM and in the dark matter are related to one another, then cross-correlating  $\kappa$  and  $\delta\mathcal{F}$  will yield a non-zero result. The measurement of these cross-correlations tests whether the IGM is tracing the underlying dark matter field and quantifies the bias between flux and matter.

## **B. The Correlators**

### *Physical Interpretation*

The two correlators  $\langle\delta\mathcal{F}\kappa\rangle$  and  $\langle\delta\mathcal{F}^2\kappa\rangle$  have substantially different physical meaning:  $\kappa$  is proportional to the

over(under)density integrated along the los and is dominated by long wavelength modes with  $k \sim 10^{-2} h \text{ Mpc}^{-1}$ . Intuitively  $\kappa$  therefore measures whether a specific los is probing an overall over(under)dense region. If the IGM traces the dark matter field, then by Eq. (3)  $\delta\mathcal{F}$  is expected to measure the dark matter overdensity along the same los extending over the redshift range  $\Delta z$  spanned by the QSO spectrum. This implies that

- $\langle\delta\mathcal{F}\kappa\rangle$  quantifies whether and how much the overdensities traced by the Lyman- $\alpha$  flux contribute to the overall overdensity measured all the way to the last scattering surface. Because both  $\kappa$  and  $\delta\mathcal{F}$  are proportional to  $\delta$ , it is reasonable to expect that this correlator will be dominated by modes with wavelengths of the order of hundreds of comoving Mpc. As such, this correlator may be difficult to measure as it may be more sensitive to the calibration of the Lyman- $\alpha$  forest continuum.
- $\langle\delta\mathcal{F}^2\kappa\rangle$  measures the relationship between long wavelength modes in the density and the amplitude of the variance of the flux. The variance on small scales and the amplitude of fluctuations on large-scales are not coupled in linear theory. However, in non-linear gravitational theory regions of higher mean density have higher matter fluctuations. These lead to higher amplitude fluctuations in flux [39]. Since  $\langle\delta\mathcal{F}^2\kappa\rangle$  is sensitive to this interplay between long and short wavelength modes, this correlator is much more sensitive than  $\langle\delta\mathcal{F}\kappa\rangle$  to the structure growth rate. Furthermore, because  $\delta\mathcal{F}^2$  is sensitive to short wavelengths, this signal is dominated by modes with shorter wavelength than the ones dominating  $\langle\delta\mathcal{F}\kappa\rangle$ . As such, this signal should be less sensitive to the fitting of the continuum of the Lyman- $\alpha$  forest.

### *Tree level approximation*

In what follows we focus on obtaining analytic expressions for the correlations between the (variance of the) flux fluctuations in the Lyman- $\alpha$  spectrum and the CMB convergence  $\kappa$  measured along the same los. From Eqs. (3, 4) above it is straightforward to obtain the general expression for the signal

$$\begin{aligned} \langle\delta\mathcal{F}^r(\hat{n})\kappa(\hat{n})\rangle &= \frac{3H_0^2\Omega_m}{2c^2} \int_0^{\chi_F} d\chi_c \frac{W_L(\chi_c, \chi_F)}{a(\chi_c)} \\ &\times \int_{\chi_i}^{\chi_Q} d\chi_q (-A\beta)^r \langle\delta^r(\hat{n}, \chi_q) \delta(\hat{n}, \chi_c)\rangle. \end{aligned} \quad (5)$$

Since the QSOs used to measure the Lyman- $\alpha$  forest lie at  $z > 2$ , it is reasonable to expect that non-linearities induced by gravitational collapse will not have a large impact on the final results. In the following we therefore calculate the  $r = 1$  and  $r = 2$  correlators at *tree-level*

in cosmological perturbation theory. While beyond the scope of the current calculation, we could include the effects of non-linearities induced by gravitational collapse by applying the *Hyperextended Perturbation Theory* of Ref. [40] to the terms in Eq. (5).

At tree level in perturbation theory the redshift dependence of the matter power spectrum factorizes into  $P(k, \chi_c, \chi_q) = P_L(k) D(\chi_c) D(\chi_q)$ , where  $P_L(k)$  denotes the zero-redshift linear power spectrum and  $D(\chi)$  the growth factor at comoving distance  $\chi$ . Furthermore, the correlator appearing in the integrand of Eq. (5) depends on the separation  $\Delta\chi = \chi_q - \chi_c$  between the two points running on the los and in general it will be significantly non-zero only when  $|\Delta\chi| \leq \Delta\chi_0 \approx 150 h^{-1} \text{Mpc}$ . Also, at tree level in perturbation theory these correlators carry  $2r$  factors of  $D$ .<sup>1</sup> Using the approximation

$$D(\chi_c) = D(\chi_q - \Delta\chi) \approx D(\chi_q), \quad (6)$$

$$W_L(\chi_c, \chi_F) = W_L(\chi_q - \Delta\chi, \chi_F) \approx W_L(\chi_q, \chi_F), \quad (7)$$

$$a(\chi_c) = a(\chi_q - \Delta\chi) \approx a(\chi_q), \quad (8)$$

we can then write  $\langle \delta^r(\hat{n}, \chi_q) \delta(\hat{n}, \chi_c) \rangle \approx \xi_r(\Delta\chi) D^{2r}(\chi_q)$  and trade the double integration (over  $\chi_c$  and  $\chi_q$ ) for the product of two single integrations over  $\Delta\chi$  and  $\chi_q$ . Equation (5) factorizes into

$$\begin{aligned} \langle \delta \mathcal{F}^r \kappa \rangle &\approx (-A\beta)^r \frac{3H_0^2 \Omega_m}{2c^2} \int_{\chi_i}^{\chi_q} d\chi_q \frac{W_L(\chi_q, \chi_F)}{a(\chi_q)} D^{2r}(\chi_q) \\ &\times \int_{-\Delta\chi_0}^{\Delta\chi_0} d\Delta\chi \xi_r(\Delta\chi). \end{aligned} \quad (9)$$

This is the expression used to evaluate the signal. The determination of an expression for  $\xi_r$  and of an efficient way for evaluating it is the focus of the rest of the section.

### Window Functions

The experiments that measure the convergence and the flux fluctuations have finite resolutions. We approximate the effective window functions of these experiments by analytically tractable Gaussian function.

These two window functions act differently: the finite resolution of the CMB convergence measurements limits the accessible range of modes perpendicular to the los,  $\vec{k}_\perp$ , and the finite resolution of the Lyman- $\alpha$  spectrum limits the range of accessible modes  $k_\parallel$  parallel to the los. This separation of the modes into the ones parallel and perpendicular to the los is intrinsically dictated by the nature of the observables and it cannot be avoided once the finite resolution of the various observational

campaigns is taken into account. Because of this symmetry, the calculation is most transparent in cylindrical coordinates:  $\vec{k} = k_\parallel \hat{n} + \vec{k}_\perp$ .

The high- $k$  (short wavelength) cutoff scales for the CMB and Lyman- $\alpha$  modes are denoted by  $k_C$  and  $k_L$  respectively. Furthermore, we also add a low- $k$  (long wavelength) cutoff for the Lyman- $\alpha$  forest, to take into account the fact that wavelengths longer than the spectrum will appear in the spectrum itself as a background. We denote this low- $k$  cutoff by  $k_l$ . After defining the auxiliary quantities

$$\bar{k}^2 \equiv \frac{k_L^2 k_l^2}{k_L^2 + k_l^2}, \quad (10)$$

$$\hat{k}^2 \equiv \frac{k_L^2 k_l^2}{2k_l^2 + k_L^2}, \quad (11)$$

the window functions acting on the Lyman- $\alpha$  and on the CMB modes, denoted respectively by  $W_\alpha$  and  $W_\kappa$ , are defined through

$$\begin{aligned} W_\alpha(k_\parallel, k_L, k_l) &\equiv \left[ 1 - e^{-(k_\parallel/k_l)^2} \right] e^{-(k_\parallel/k_L)^2} \\ &= e^{-(k_\parallel/k_L)^2} - e^{-(k_\parallel/\bar{k})^2}, \end{aligned} \quad (12)$$

$$W_\kappa(\vec{k}_\perp, k_C) \equiv e^{(-\vec{k}_\perp^2/k_C^2)}, \quad (13)$$

where the direction dependence of the two window functions has been made explicit.

We determine the values of the cutoff scales as follows. For the Lyman- $\alpha$  forest, we consider the limitations imposed by the spectrograph, adopting the two cutoff scales  $k_L$  and  $k_l$  according to the observational specifications. For the reconstruction of the CMB convergence map we compute the minimum variance lensing reconstruction noise following Hu and Okamoto [41]. We then identify the multipole  $l_c$ , where the signal power spectrum equals the noise power spectrum for the reconstructed deflection field (for  $l > l_c$  the noise is higher than the signal). Finally, we translate the angular cutoff  $l_c$  into a 3-D Fourier mode  $k_C$  at the relevant redshift so to keep only modes with  $k \leq k_C$  in the calculation. Note that if we had used the shape of the noise curve instead of this Gaussian cutoff, we would have effectively retained more Fourier modes, thereby increasing the signal. However, to keep the calculations simple and conservative we use the above Gaussian window. In what follows, we will present results for convergence map reconstructions from the datasets of two CMB experiments: Planck and an hypothetical CMB polarization experiment based on a proposed new camera for the Atacama Cosmology Telescope (ACTPOL). For the former, we adopt the sensitivity values of the 9 frequency channels from the Blue Book [42]. For the latter we assume a hypothetical polarization based CMB experiment with a 3 arcmin beam and 800 detectors, each having a noise-equivalent-temperature (NET) of  $300 \mu\text{K}\sqrt{s}$  over 8000 sq. deg., with an integration time of  $3 \times 10^7$  seconds. We further assume that both experiments will completely cover the 8000 sq. deg footprint of BOSS.

<sup>1</sup> Notice in fact that even though in the  $r = 2$  case it would be reasonable to expect three factors of  $D$ , the first non-zero contribution to the three-point function carries four factors of  $D$  because the gaussian term vanishes exactly.



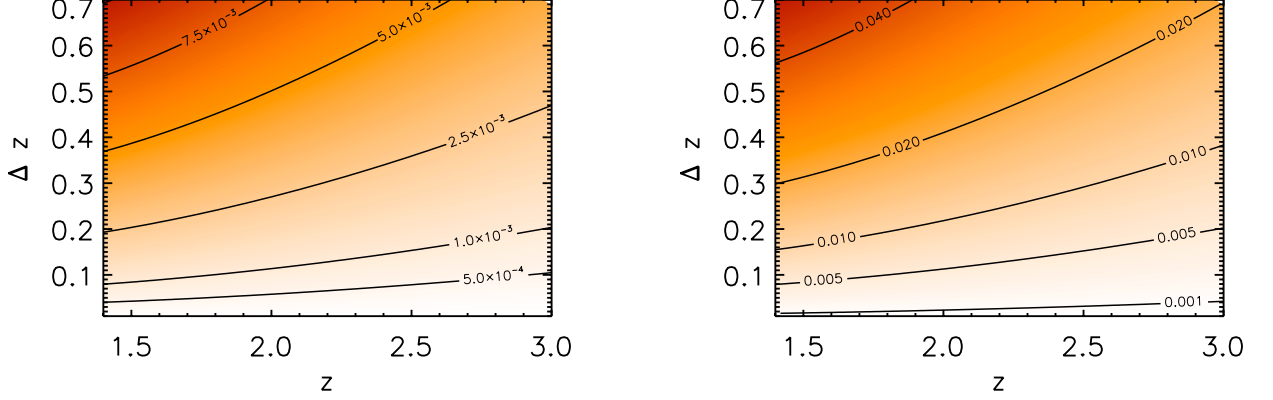


FIG. 1: Absolute value of the correlator  $\langle \delta \mathcal{F} \kappa \rangle$  along a *single* line-of-sight as a function of the source redshift  $z$  and of the length of the measured spectrum  $\Delta z$ , for convergence maps reconstructed from Planck (left panel,  $k_C = 0.021 h \text{ Mpc}^{-1}$ ) and ACTPOL (right panel,  $k_C = 0.064 h \text{ Mpc}^{-1}$ ). The value of the resolution of the QSO spectrum is the one predicted for SDSS-III,  $k_L = 4.8 h \text{ Mpc}^{-1}$ . To make the physics of structure formation apparent, we turn off the IGM physics by setting  $A = \beta = 1$  (it is straightforward to rescale the values of the correlator to reflect different values of  $A$  and  $\beta$ ).

### Auxiliary Functions

Because the calculation has cylindrical rather than spherical symmetry, the evaluation of the correlators of Eq. (9) is more complicated, particularly for  $r > 1$ . As shown in the appendix, it is possible to step around this complication and to obtain results that are computation-

ally efficient with the adoption of a few auxiliary functions that allow the integrations in  $k$ -space to be carried out in two steps, first integrating on the modes perpendicular to the los, and subsequently on the ones parallel to the los. The perturbative results for the correlators are expressed as combinations of the following auxiliary functions:

$$\tilde{H}_m(k_{\parallel}; k_C) \equiv \int_{|k_{\parallel}|}^{\infty} \frac{k dk}{2\pi} \frac{P_L(k)}{m!} \left( \frac{k^2 - k_{\parallel}^2}{k_C^2} \right)^m \exp \left( -\frac{k^2 - k_{\parallel}^2}{k_C^2} \right), \quad (14)$$

$$\tilde{L}_m(k_{\parallel}; k_C) \equiv \int_{|k_{\parallel}|}^{\infty} \frac{dk}{2\pi k} \frac{P_L(k)}{m!} \left( \frac{k^2 - k_{\parallel}^2}{k_C^2} \right)^m \exp \left( -\frac{k^2 - k_{\parallel}^2}{k_C^2} \right), \quad (15)$$

$$f_m^{(n)}(\Delta\chi; k_C, k_L) \equiv \int_{-\infty}^{\infty} \frac{dk_{\parallel}}{2\pi} \left( \frac{k_{\parallel}}{k_L} \right)^n \exp \left[ -\frac{k_{\parallel}^2}{k_L^2} + i k_{\parallel} \Delta\chi \right] \tilde{f}_m(k_{\parallel}; k_C) \quad \text{with } f = \{L, H\}, \quad (16)$$

$$\tilde{f}_0^{(n)}(s) \equiv \int_{-\infty}^{\infty} \frac{dk}{2\pi} \left( \frac{k}{s} \right)^n \left[ e^{-2k^2/s^2} - e^{-k^2/\hat{k}^2} \right] \tilde{f}_0(k; \infty) \quad \text{with } f = \{L, H\}. \quad (17)$$

Equations (14) and (15) above represent an intermediate step, where the integration on the modes perpendicular to the los is carried out. Equations (16) and (17) are then used to carry out the remaining integration over the modes that are parallel to the los.

The symmetry properties of the auxiliary functions are as follows. The functions  $\tilde{f}_m$  are *real and even* in  $k_{\parallel}$  regardless of the actual value of  $m$ . This in turn implies that  $f_m^{(n)}$  are real and even (imaginary and odd) in  $\Delta\chi$

when  $n$  is even (odd). Furthermore, the coefficients  $\tilde{f}_0^{(n)}$  are real and non-zero only if  $n$  is even, thus ensuring that  $\xi_r(\Delta\chi)$  is always real-valued.

### The $\langle \delta \mathcal{F} \kappa \rangle$ correlator

In the  $r = 1$  case it is straightforward to identify  $\xi_1(\Delta\chi)$  with a two point correlation function measured along the los. However, the intrinsic geometry of the

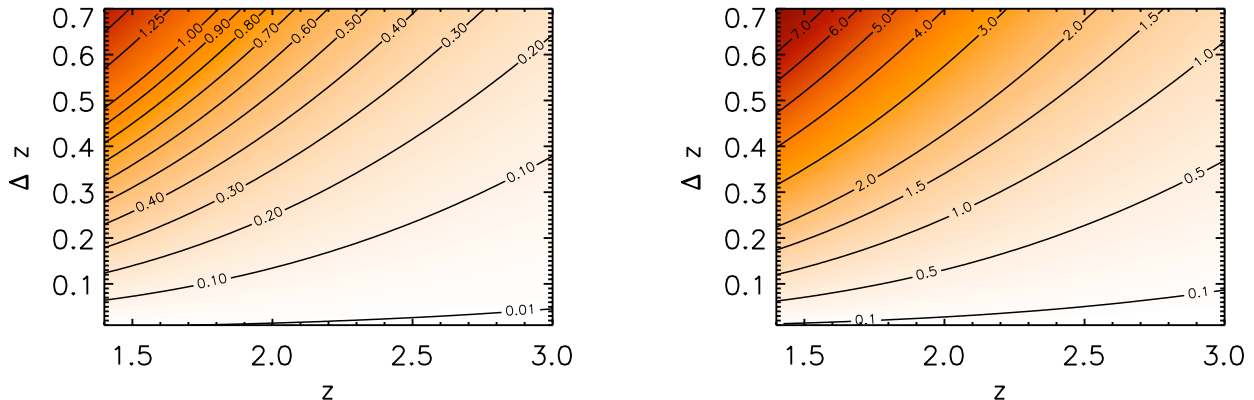


FIG. 2: Absolute value of the correlator  $\langle \delta \mathcal{F}^2 \kappa \rangle$  along a *single* line-of-sight as a function of the source redshift  $z$  and of the length of the measured spectrum  $\Delta z$ , for convergence maps reconstructed from Planck (left panel,  $k_C = 0.021 h \text{ Mpc}^{-1}$ ) and ACTPOL (right panel,  $k_C = 0.064 h \text{ Mpc}^{-1}$ ). The value of the resolution of the QSO spectrum is the one predicted for SDSS-III,  $k_L = 4.8 h \text{ Mpc}^{-1}$ . As before, we set  $A = \beta = 1$  to make the physics of structure formation apparent.

problem and the inclusion of the window functions leads to evaluate this correlation function in a way that is different from the usual case, where the spherical symmetry in  $k$ -space can be exploited. In the present case we have

$$\xi_1(\Delta\chi) = H_0^{(0)}(\Delta\chi; k_C, k_L) - H_0^{(0)}(\Delta\chi; k_C, \bar{k}). \quad (18)$$

It is then straightforward to plug Eq. (18) into Eq. (9) to obtain  $\langle \delta \mathcal{F}(\hat{n}) \kappa(\hat{n}) \rangle$ .<sup>2</sup> In Fig. 1 we show the absolute value of the cross-correlation of the convergence  $\kappa$  of the CMB with the Lyman- $\alpha$  flux fluctuations  $\delta \mathcal{F}$  observed for a quasar located at redshift  $z$  and whose spectrum spans a range of redshift  $\Delta z$ . The cosmological model used (and assumed throughout this work) is a flat  $\Lambda$ CDM universe with  $\Omega_m = 0.25$ ,  $h = 0.72$  and  $\sigma_8 = 0.84$  consistent with the WMAP-5 cosmology [12]. The left and right panel show the results for the resolution of Planck and of the proposed ACTPOL experiment. We artificially set  $A = \beta = 1$ , effectively “turning off” the physics of IGM: this choice is not dictated by any physical argument but from the fact that it makes apparent the dynamics of structure formation.

The behavior of  $\langle \delta \mathcal{F} \kappa \rangle$  shown in Fig. 1 makes physical sense. Recall that this correlator is sensitive to

the overdensity integrated along the redshift interval  $\Delta z$  (spanned by the QSO spectrum) that contributes to the CMB convergence. It then increases almost linearly with the length of the QSO spectrum  $\Delta z$ . It also increases if the resolution of the CMB experiment  $k_C$  is increased. An increased value of  $\Delta z$  corresponds to a longer Lyman- $\alpha$  spectrum, carrying a larger amount of information and thus leading to a larger correlation. Similarly, an increased value of  $k_C$  corresponds to a higher resolution of the reconstructed convergence map and therefore more modes – and information – being included in the correlation. Deepening the source’s redshift (while keeping  $A$  and  $\beta$  fixed) on the other hand results in a *decrease* in  $\langle \delta \mathcal{F} \kappa \rangle$ . This fact is related to the growth of structure: the spectrum of a higher redshift QSO is probing regions where structure is less clumpy and therefore the absolute value of the correlation is smaller. Finally, once the redshift dependence of  $A$  is turned on ( $\beta$  is only mildly redshift dependent) the above result change, leading to a final signal that is increasing with redshift.

We stress here that values of the correlators will be different when  $A$  and  $\beta$  are different from unity. Ultimately these values should be recovered from a full non-linear study based on large scale-high resolution hydrodynamical simulations. However, numerical studies based on hydrodynamical simulations have shown convincingly that for both the flux power spectrum (2-pt function) and flux bispectrum (3-pt function) the shape is very similar to the matter power and bispectrum, while the amplitude is usually matched for values of  $A$  and  $\beta$  that are different from linear predictions (see discussion in [43]). In this framework, non-linear hydrodynamical simulations should at the end provide the “effective” values for  $A$  and  $\beta$  that will match the observed correlators and our results can be recasted in terms of these new parameters in a straightforward way.

<sup>2</sup> We checked that in the limit where  $k_L \rightarrow \infty$ ,  $k_C \rightarrow \infty$  and  $k_l \rightarrow 0$  the usual two point correlation function is recovered. Whereas one would naively expect that letting  $k_L = k_C$  and  $k_l = 0$  would lead to recover the usual two point function calculated exploiting spherical symmetry in  $k$ -space with a cutoff scale equal to the common  $k_L$ , this is actually *not* the case. The reason for this is that the volume of  $k$ -space over which the integration is carried out is different for the two choices of coordinate systems. In particular, the spherical case always includes fewer modes than the cylindrical one. The two results therefore coincide *only* in the  $k_L \rightarrow \infty$  limit.

*The  $\langle \delta \mathcal{F}^2 \kappa \rangle$  correlator*

The  $r = 2$  case, where the variance of the flux fluctuation  $\delta \mathcal{F}^2$  integrated along the los is cross-correlated with  $\kappa$ , is more involved. Looking back at Eqs. (5, 9) it is possible to realize that the cumulant correlator  $\langle \delta^2(\hat{n}, \chi_q) \delta(\hat{n}, \chi_c) \rangle = \xi_2(\Delta\chi)$  corresponds to a collapsed three-point correlation function, as two of the  $\delta$ 's refer to the same physical point. The evaluation of  $\xi_2$  is complicated by the introduction of the window functions  $W_\alpha$

and  $W_\kappa$ . For sake of clarity, we report here only the final results at tree level in cosmological perturbation theory, relegating the lengthy derivation to the appendix. Letting

$$\xi_2(\Delta\chi) = \langle \delta_q^2 \delta_c \rangle_{1,2} + 2 \langle \delta_q^2 \delta_c \rangle_{2,3}, \quad (19)$$

and using the auxiliary functions defined in Eqs. (14-17) above, it is possible to obtain the following series solution

$$\begin{aligned} \langle \delta^2 \delta \rangle_{1,2} &= 2 \sum_{m=0}^{\infty} \left\{ \frac{5}{7} \left[ H_m^{(0)}(\Delta\chi, \chi_q; k_C, k_L) - H_m^{(0)}(\Delta\chi, \chi_q; k_C, \bar{k}) \right]^2 \right. \\ &\quad + \left[ k_L H_m^{(1)}(\Delta\chi, \chi_q; k_C, k_L) - \bar{k} H_m^{(1)}(\Delta\chi, \chi_q; k_C, \bar{k}) \right] \left[ k_L L_m^{(1)}(\Delta\chi, \chi_q; k_C, k_L) - \bar{k} L_m^{(1)}(\Delta\chi, \chi_q; k_C, \bar{k}) \right] \\ &\quad - m k_C^2 \left[ H_m^{(0)}(\Delta\chi, \chi_q; k_C, k_L) - H_m^{(0)}(\Delta\chi, \chi_q; k_C, \bar{k}) \right] \left[ L_m^{(0)}(\Delta\chi, \chi_q; k_C, k_L) - L_m^{(0)}(\Delta\chi, \chi_q; k_C, \bar{k}) \right] \\ &\quad + \frac{2}{7} \left[ k_L^2 L_m^{(2)}(\Delta\chi, \chi_q; k_C, k_L) - \bar{k}^2 L_m^{(2)}(\Delta\chi, \chi_q; k_C, \bar{k}) \right]^2 \\ &\quad - \frac{4m}{7} k_C^2 \left[ k_L L_m^{(1)}(\Delta\chi, \chi_q; k_C, k_L) - \bar{k} L_m^{(1)}(\Delta\chi, \chi_q; k_C, \bar{k}) \right]^2 \\ &\quad \left. + \frac{m(2m-1)}{7} k_C^4 \left[ L_m^{(0)}(\Delta\chi, \chi_q; k_C, k_L) - L_m^{(0)}(\Delta\chi, \chi_q; k_C, \bar{k}) \right]^2 \right\}, \quad (20) \end{aligned}$$

$$\begin{aligned} \langle \delta_q^2 \delta_c \rangle_{2,3} &= 2 \sum_{m=0}^{\infty} \frac{(-1)^m 2^m}{m!} \left[ \frac{6}{7} \bar{H}_0^{(m)}(k_L) H_0^{(m)}(\Delta\chi; k_C, k_L) + \frac{1}{2} k_L^2 \bar{L}_0^{(m+1)}(k_L) H_0^{(m+1)}(\Delta\chi; k_C, k_L) \right. \\ &\quad + \frac{1}{2} k_L^2 \bar{H}_0^{(m+1)}(k_L) L_0^{(m+1)}(\Delta\chi; k_C, k_L) + \frac{3}{7} k_L^4 \bar{L}_0^{(m+2)}(k_L) L_0^{(m+2)}(\Delta\chi; k_C, k_L) \\ &\quad \left. - \frac{k_L^2}{7} \bar{H}_0^{(m)}(k_L) L_0^{(m+2)}(\Delta\chi; k_C, k_L) - \frac{k_L^2}{7} \bar{L}_0^{(m+2)}(k_L) H_0^{(m)}(\Delta\chi; k_C, k_L) + (k_L \rightarrow \bar{k}) \right]. \quad (21) \end{aligned}$$

In Fig. 2 we show the result obtained using the tree level expression for  $\langle \delta \mathcal{F}^2 \kappa \rangle$ , Eqs. (19-21). As before, we focus on the physics of structure formation and we turn off the IGM physics by setting  $A = \beta = 1$ . First, it is necessary to keep in mind that  $\langle \delta \mathcal{F}^2 \kappa \rangle$  is sensitive to the interplay of long and short wavelength modes and it probes the enhanced growth of short wavelength overdensities that lie in an environment characterized by long wavelength overdensities. The behavior of  $\langle \delta \mathcal{F}^2 \kappa \rangle$  with respect to  $z$  and  $\Delta z$  is similar to that of  $\langle \delta \mathcal{F} \kappa \rangle$ : it increases if  $\Delta z$  is increased or if the QSO redshift is decreased. However, the effect of the growth of structure is in this case stronger than in the previous case. This does not come as a surprise, as the growth of structure acts coherently in two ways on  $\langle \delta \mathcal{F}^2 \kappa \rangle$ . Since in a  $\Lambda$ CDM model all modes grow at the same rate, a lower redshift for the source QSO implies larger overdensities on large scales which in turn enhance even further the growth of overdensities on small scales. Thus by lowering the source's redshift two factor play together to enhance the signal: first the fact that long and short wavelength modes have

both grown independently, and second the fact that being coupled larger long-wavelength modes boost the growth of short wavelength modes by a larger amount. This dependence is also made explicit in Eq. (9), where we note that  $\langle \delta \mathcal{F}^2 \kappa \rangle$  depends on four powers of the growth factor. Finally, as before, the higher the resolution of the CMB experiment the larger is  $d\langle \delta \mathcal{F}^2 \kappa \rangle / d\Delta z$ . This too makes physical sense, as a larger resolution leads to more modes contributing to the signal and therefore to a larger cross-correlation.

### C. Variance of correlators

To assess whether the correlations between fluctuations in the flux and convergence are detectable we need to estimate the signal-to-noise ratio, which in turn requires the evaluation of the noise associated with the above observable. As mentioned above, both instrumental noise and cosmic variance are considered. We then move to

estimate the variance of our correlator

$$\sigma_r^2 \equiv \langle \delta \mathcal{F}^{2r} \kappa^2 \rangle - \langle \delta \mathcal{F}^r \kappa \rangle^2. \quad (22)$$

Since  $\langle \delta \mathcal{F}^r \kappa \rangle^2$  is just the square of the signal, we aim here to obtain *estimates* for  $\langle \delta \mathcal{F}^{2r} \kappa^2 \rangle$ . From Eq. (5), we get:

$$\begin{aligned} \langle \delta \mathcal{F}^{2r} \kappa^2 \rangle &= \left( A^r \beta^r \frac{3H_0^2 \Omega_m}{2c^2} \right)^2 \int_0^{\chi_F} d\chi_c \frac{W_L(\chi_c, \chi_F)}{a(\chi_c)} \\ &\times \int_0^{\chi_F} d\chi'_c \frac{W_L(\chi'_c, \chi_F)}{a(\chi'_c)} \int_{\chi_i}^{\chi_Q} d\chi_q \int_{\chi_i}^{\chi_Q} d\chi'_q \\ &\times \langle \delta^r(\hat{n}, \chi_q) \delta^r(\hat{n}, \chi'_q) \delta(\hat{n}, \chi_c) \delta(\hat{n}, \chi'_c) \rangle, \quad (23) \end{aligned}$$

where there are now two integrals running along the convergence los (on  $\chi_c$  and  $\chi'_c$ ) and two running along the Lyman- $\alpha$  spectrum (on  $\chi_q$  and  $\chi'_q$ ). The correlator appearing in the integrand of Eq. (23) is characterized by an even  $(2r+2)$  number of  $\delta$  factors. This implies that an approximation to its value can be obtained using Wick's theorem. When Wick's theorem is applied, many different terms will in general appear. Adopting for sake of brevity the notation  $\delta(\hat{n}, \chi'_i) \equiv \delta_i$ , terms characterized by the contraction of  $\delta_i$  and  $\delta_j$  will receive non-negligible contributions over the overlap of the respective los. The terms providing the largest contribution to  $\langle \delta \mathcal{F}^{2r} \kappa^2 \rangle$  are the ones where  $\delta_c$  is contracted with  $\delta_{c'}$ : these terms in fact contain the value of the cosmic variance of the convergence and receive significant contributions from all points along the los from the observer all the way to the last scattering surface. On the other hand, whenever we consider the cross-correlation between a  $\delta_c$  and a  $\delta_q$ , this will acquire a non-negligible value only for those set of points where the los to the last scattering surface overlaps with the Lyman- $\alpha$  spectrum. As such, these terms are only proportional to the length of the Lyman- $\alpha$  spectrum, and thus sensibly smaller than the ones containing the variance of the convergence. We note in passing that the same argument should also apply to the connected part of the correlator, which should be significantly non-zero only along the Lyman- $\alpha$  spectrum. Mathematically, these facts become apparent from Eq. (23) above, where terms containing  $\langle \delta_c \delta_{c'} \rangle$  are the only ones for which the integration over  $\chi_c$  and  $\chi'_c$  can be traded for an integration over  $\Delta\chi_c$  and an integration over  $\chi_c$  that extends *all the way to*  $\chi_F$ . If on the other hand  $\delta_c$  is contracted with a  $\delta_q$  factor, then the approximation scheme of Eqs. (6-8) leads to an integral over  $\Delta\chi$  and to an integral over  $\chi_q$  that extends only over the length probed by the Lyman- $\alpha$  spectrum. It seems therefore possible to safely neglect terms where the  $\delta$ 's referring to the convergence are not contracted with each other.

#### The variance of $\delta \mathcal{F} \kappa$

We start by considering the variance of  $\delta \mathcal{F} \kappa$ . Setting  $r = 1$  in Eq. (23) and using Wick's theorem we obtain

$$\langle \delta_q \delta_{q'} \delta_c \delta_{c'} \rangle \approx 2 \langle \delta_q \delta_c \rangle \langle \delta_{q'} \delta_{c'} \rangle + \langle \delta_q \delta_{q'} \rangle \langle \delta_c \delta_{c'} \rangle. \quad (24)$$

We notice immediately that the first term is twice the square of  $\langle \delta \mathcal{F} \kappa \rangle$ , while the second term is proportional to two correlation function characterized by cutoffs acting *either* on the modes that are parallel *or* perpendicular to the los, *but not on both*. It is then possible to show that

$$\begin{aligned} \langle \delta_q \delta_{q'} \rangle &= D(\chi_q) D(\chi_{q'}) \left[ H_0^{(0)}(\Delta\chi_q; \infty, k_L/\sqrt{2}) \right. \\ &\quad \left. - H_0^{(0)}(\Delta\chi_q; \infty, \bar{k}/\sqrt{2}) \right], \quad (25) \end{aligned}$$

$$\langle \delta_c \delta_{c'} \rangle = D(\chi_c) D(\chi_{c'}) H_0^{(0)}(\Delta\chi_c; k_C/\sqrt{2}, \infty), \quad (26)$$

$$\begin{aligned} \langle \delta_q \delta_c \rangle &= D(\chi_c) D(\chi_q) \\ &\times \left[ H_0^{(0)}(\Delta\chi; k_C, k_L) - H_0^{(0)}(\Delta\chi; k_C, \bar{k}) \right], \quad (27) \end{aligned}$$

$$\langle \delta_q^2 \rangle = D^2(\chi_q) \left[ \bar{H}_0^{(0)}(\chi_q, k_L) + \bar{H}_0^{(0)}(\chi_q, \bar{k}) \right], \quad (28)$$

where the last two equations have been added here for sake of completeness, as they will be useful in what follows. The variance of  $\delta \mathcal{F} \kappa$  is then

$$\begin{aligned} \sigma_1^2 &\approx \langle \delta \mathcal{F} \kappa \rangle^2 \\ &+ \left( A\beta \frac{3H_0^2 \Omega_m}{2c^2} \right)^2 \int_0^{\chi_F} d\chi_c \frac{W_L^2(\chi_c, \chi_F)}{a^2(\chi_c)} D^2(\chi_c) \\ &\times \int_{\chi_i}^{\chi_Q} d\chi_q D^2(\chi_q) \int_{-\Delta\chi_{c,0}}^{\Delta\chi_{c,0}} d\Delta\chi_c H_0^{(0)}(\Delta\chi_c; k_C/\sqrt{2}, \infty) \\ &\times \int_{-\Delta\chi_{q,0}}^{\Delta\chi_{q,0}} d\Delta\chi_q \left[ H_0^{(0)}(\Delta\chi_q; \infty, k_L/\sqrt{2}) \right. \\ &\quad \left. - H_0^{(0)}(\Delta\chi_q; \infty, \bar{k}/\sqrt{2}) \right]. \quad (29) \end{aligned}$$

In the upper panels of Fig. 3 we show the values obtained for the *standard deviation* of  $\delta \mathcal{F} \kappa$  for two different CMB experiments' resolution, again turning off the IGM physics evolution and focusing on the growth of structure.

#### The variance of $\delta \mathcal{F}^2 \kappa$

Setting  $r = 2$  in Eq. (23), we then apply Wick's theorem to  $\langle \delta_q^2 \delta_{q'}^2 \delta_c \delta_{c'} \rangle$ . Neglecting again terms where the  $\delta_c$ 's are not contracted with one another, we obtain

$$\begin{aligned} \langle \delta_q^2 \delta_{q'}^2 \delta_c \delta_{c'} \rangle &\approx 2 \langle \delta_q^2 \delta_c \rangle \langle \delta_{q'}^2 \delta_{c'} \rangle \\ &+ \langle \delta_c \delta_{c'} \rangle \left( \langle \delta_q^2 \rangle \langle \delta_{q'}^2 \rangle + 2 \langle \delta_q \delta_{q'} \rangle^2 \right), \quad (30) \end{aligned}$$



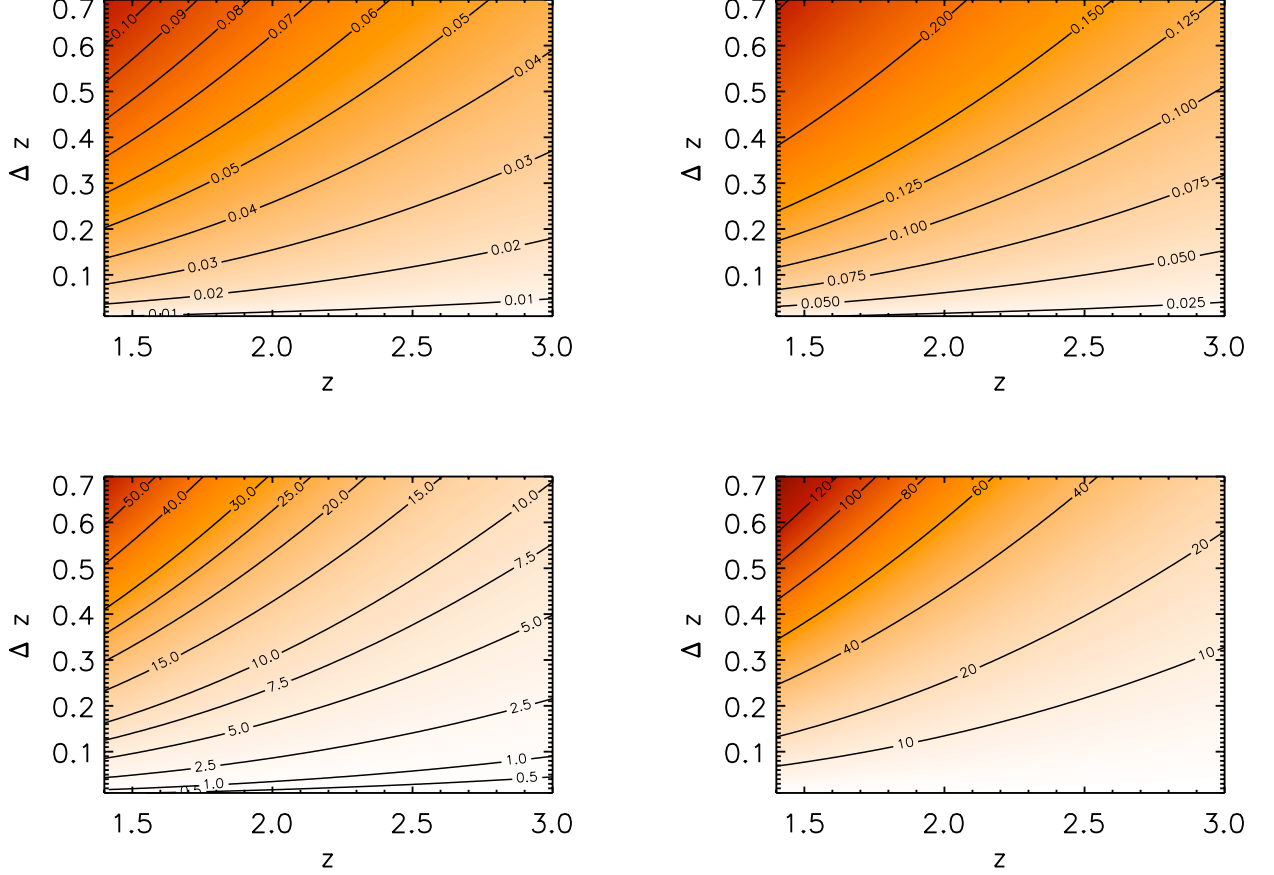


FIG. 3: Estimates of the standard deviation of the correlator  $\delta\mathcal{F}\kappa$  (upper panels) and  $\delta\mathcal{F}^2\kappa$  (lower panels) along a *single* line-of-sight as a function of the source redshift  $z$  and of the length of the measured spectrum  $\Delta z$ , for convergence maps reconstructed from Planck (left panels) and ACTPOL (right panels). As before, we set  $A = \beta = 1$ , effectively turning off the physics of IGM, to make apparent the physics of structure formation.

which then leads to the expression for  $\sigma_2^2$

$$\begin{aligned}
 \sigma_2^2 &\approx \langle \delta\mathcal{F}^2\kappa \rangle^2 \\
 &+ \left( A\beta \frac{3H_0^2\Omega_m}{2c^2} \right)^2 \int_0^{\chi_F} d\chi_c \frac{W_L^2(\chi_c, \chi_F)}{a^2(\chi_c)} D^2(\chi_c) \\
 &\times \int_{-\Delta\chi_{c,0}}^{\Delta\chi_{c,0}} d\Delta\chi_c H_0^{(0)}(\Delta\chi_c; k_C/\sqrt{2}, \infty) \\
 &\times \left\{ \left[ \bar{H}_0^{(0)}(\chi_q, k_L) + \bar{H}_0^{(0)}(\chi_q, \bar{k}) \right]^2 \left[ \int_{\chi_i}^{\chi_Q} d\chi_q D^2(\chi_q) \right]^2 \right. \\
 &+ 2 \int_{\chi_i}^{\chi_Q} d\chi_q D^4(\chi_q) \int_{-\Delta\chi_{q,0}}^{\Delta\chi_{q,0}} d\Delta\chi_q \left[ H_0^{(0)}(\Delta\chi_q; \infty, k_L/\sqrt{2}) \right. \\
 &\left. \left. - H_0^{(0)}(\Delta\chi_q; \infty, \bar{k}/\sqrt{2}) \right]^2 \right\}. \quad (31)
 \end{aligned}$$

In the lower panels of Fig. 3 we show the estimates for the *standard deviation*  $\delta\mathcal{F}^2\kappa$  along a *single* line-of-sight for the two different CMB experiment. We note in Fig. 3 the same trends that have been pointed out for the

correlator itself in Fig. 1 and 2: the standard deviation of  $\delta\mathcal{F}\kappa$  and of  $\delta\mathcal{F}^2\kappa$  increase almost linearly with increasing length of the Lyman- $\alpha$  spectrum  $\Delta z$  and it decreases as the source redshift  $z$  is increased because of the fact that the spectrum probes regions that are less clumpy. Also, by increasing the resolution of the CMB experiment used to reconstruct the convergence map, the deviation of  $\delta\mathcal{F}\kappa$  and  $\delta\mathcal{F}^2\kappa$  also increase: if on one hand more modes carry more information, on the other hand they also carry more cosmic variance.

One last aspect to note here is that while the signal for  $\langle \delta\mathcal{F}^2\kappa \rangle$  arises from a three point correlation function (which in the gaussian approximation would yield zero), the dominant terms contributing to its variance arise from products of two point correlation functions. In particular, it is possible to show that the terms appearing in the second line of Eq. (30) significantly outweigh the square of the signal that appears in the first line.



CMB Exp.	S/N per <i>los</i>	Total S/N in BOSS	Total S/N in BigBOSS
Planck	0.075	30	75
ACTPOL	0.130	52	130

TABLE I: Estimates of the total and per single *los* signal-to-noise (S/N) of the  $\langle\delta\mathcal{F}\kappa\rangle$  cross-correlation for different CMB experiments combined with BOSS and BigBOSS.

surements. As expected, while the S/N for  $\langle\delta\mathcal{F}\kappa\rangle$  does not show any strong redshift dependence, the S/N for  $\langle\delta\mathcal{F}^2\kappa\rangle$  decreases linearly with increasing source redshift: the growth of structure is indeed playing a role and shows that QSOs lying at lower redshift will yield a larger S/N. Also, in both cases an increase in the resolution of the experiment measuring the convergence field translates in a larger S/N and in a larger derivative of the S/N with respect to  $\Delta z$ . This is not surprising, as it is reasonable to expect that a higher resolution convergence map will be carrying a larger amount of information about the density field.

All this suggests that depending on what is the correlator that one is interested in measuring, different strategies should be pursued. In case of  $\langle\delta\mathcal{F}\kappa\rangle$  increasing the length of the spectra will provide a better S/N. In case of  $\langle\delta\mathcal{F}^2\kappa\rangle$ , however, Fig. (4) suggests that an increase in the number of quasar will be more effective in producing a large S/N, whereas an increase in the redshift range spanned by the spectrum will increase the S/N only marginally.

Having obtained the S/N per *los*, we can then estimate the total S/N that will be obtained by cross-correlating the BOSS sample ( $1.6 \cdot 10^5$  QSOs) and the proposed BigBOSS sample [10] ( $10^6$  QSOs) with the convergence map measured by Planck or by the proposed ACTPOL experiment considered. Assuming a mean QSO redshift of  $\bar{z} = 2.5$  and a mean Lyman- $\alpha$  spectrum length of  $\Delta z = 0.5$ , a rough estimate of the S/N for the measurements of  $\langle\delta\mathcal{F}\kappa\rangle$  and of  $\langle\delta\mathcal{F}^2\kappa\rangle$  are given in Tab. I and II.

It is necessary to point out here that despite that the value of the S/N for  $\langle\delta\mathcal{F}\kappa\rangle$  is almost three times larger than the one for  $\langle\delta\mathcal{F}^2\kappa\rangle$ , the actual measurement of the former correlator strongly depends on the ability of fitting the continuum of the Lyman- $\alpha$  spectrum. The  $\langle\delta\mathcal{F}^2\kappa\rangle$  correlator, on the other hand, is sensitive to the interplay between long and short wavelength modes and as such should be less sensitive to the continuum fitting procedure. Therefore, even if it is characterized by a lower S/N, it may actually be the easier to measure in practice. The numbers obtained above are particularly encouraging since the S/N values are typically very large and well above unity.

CMB Exp.	S/N per <i>los</i>	Total S/N in BOSS	Total S/N in BigBOSS
Planck	0.024	9.6	24
ACTPOL	0.05	20.0	50

TABLE II: Estimates of the total and per single *los* signal-to-noise (S/N) of the  $\langle\delta\mathcal{F}^2\kappa\rangle$  cross-correlation for different CMB experiments combined with BOSS and BigBOSS.

## E. Analysis

Having developed a calculation framework for estimating  $\langle\delta\mathcal{F}\kappa\rangle$  and the S/N for their measurement, we turn to estimate what is the range of Lyman- $\alpha$  wavelengths contributing to the signal and what is the effect of changing the parameters that control the experiments' resolution.

### Spectral Analysis

We investigate here how the different Lyman- $\alpha$  modes contribute to the correlators. This should tell us whether long wavelength modes have any appreciable effect on our observables and what is the impact of short and very short wavelength modes (in particular the ones that are expected to have entered the non-linear regime).

Since the mean flux  $\bar{\mathcal{F}}$  appearing in the definition of the flux fluctuation  $\delta\mathcal{F} = (\mathcal{F} - \bar{\mathcal{F}})/\bar{\mathcal{F}}$  is a *global* quantity which is usually estimated from a statistically significant sample of high resolution QSO spectra (see the discussion in [44] for the impact that such quantity has on some derived cosmological parameters),  $\delta\mathcal{F}$  is sensitive also to modes with wavelengths longer than the Lyman- $\alpha$  spectrum. These modes appear as a “background” in each spectra but they still have to be accounted for when crosscorrelating  $\delta\mathcal{F}$  with  $\kappa$  because the fluctuation in the flux is affected by them. More specifically, a QSO that is sitting in an overdense region that extends beyond the redshift range spanned by its spectrum will see its flux decremented by a factor that in its spectrum will appear as *constant* decrement. On the other hand, if the QSO spectrum extends beyond the edge of such overdensity, this mode would appear as a fluctuation (and not as a background) in the spectrum. This extreme scenario is somewhat mitigated by the fact that present and future QSO surveys will have many QSOs with *los* separated by few comoving Mpc [45]: as such, fluxes from neighboring QSO lying in large overdense regions should present similarities that should in principle allow to detect such large overdensities in 3D tomographical studies [30].

To measure the contributions of the different modes to the correlators, we vary  $k_l$  and  $k_L$  to build appropriate filters. As can be seen from Fig. 5, where three such filters are plotted for  $\{k_l = 0.001, k_L = 0.01\}$ ,  $\{k_l = 0.01, k_L = 0.1\}$  and  $\{k_l = 0.1, k_L = 1\}$ , the gaussian

$k_l$	$k_L$	$ \langle \delta \mathcal{F} \kappa \rangle $	$\sigma_{\delta \mathcal{F} \kappa}$	Ratio
1.00e-04	1.00e-03	1.66e-04	1.77e-04	9.39e-01
1.00e-03	1.00e-02	1.20e-03	1.21e-03	9.87e-01
1.00e-02	1.00e-01	2.12e-04	6.29e-04	3.37e-01
1.00e-01	1.00e+00	6.11e-07	1.42e-03	4.30e-04
1.00e+00	1.00e+01	7.26e-08	2.44e-03	2.97e-06

TABLE III: Contribution of the different wavenumbers (split over decades) to the absolute value of the correlator  $\langle \delta \mathcal{F} \kappa \rangle$ , its standard deviation  $\sigma_{\delta \mathcal{F} \kappa}$  and ratio of the two quantities. In this calculation we took into account the evolution of  $A$  with redshift.

functional form assumed for the window function does not provide very sharp filters (hence this spectral analysis will not reach high resolution). Also, if  $k_L = 10 k_l$  then the filters add exactly to one. This allows us to measure the contributions of the different wavenumber decades to the correlators and its standard deviation.

Table III and IV summarize the results for  $\langle \delta \mathcal{F} \kappa \rangle$  and  $\langle \delta \mathcal{F}^2 \kappa \rangle$  respectively. Considering  $\langle \delta \mathcal{F} \kappa \rangle$  we note immediately that the signal and the S/N ratio both peaks around  $k \simeq 10^{-2} h \text{ Mpc}^{-1}$ , as expected from the fact that this signal is proportional to the two point correlation function, which in turn receives its largest contribution from the wavelengths that dominate the power spectrum: isolating the long wavelength modes of the Lyman- $\alpha$  flux would allow to increase the S/N. However, this procedure is sensibly complicated by the continuum fitting procedures that are needed to correctly reproduce the long

$k_l$	$k_L$	$\langle \delta \mathcal{F}^2 \kappa \rangle$	$\sigma_{\delta \mathcal{F}^2 \kappa}$	Ratio
1.00e-04	1.00e-03	1.08e-04	2.18e-02	4.99e-03
1.00e-03	1.00e-02	6.69e-03	1.96e-01	3.40e-02
1.00e-02	1.00e-01	5.92e-02	1.31e+00	4.52e-02
1.00e-01	1.00e+00	3.39e-01	7.06e+00	4.80e-02
1.00e+00	1.00e+01	9.92e-01	2.07e+01	4.79e-02

TABLE IV: Contribution of the different wavenumbers (split over decades) to the correlator  $\langle \delta \mathcal{F}^2 \kappa \rangle$ , its standard deviation  $\sigma_{\delta \mathcal{F}^2 \kappa}$  and ratio of the two quantities. In this calculation we took into account the evolution of  $A$  with redshift.

wavelength fluctuations of the Lyman- $\alpha$  flux. The behavior of the variance is interesting, as in the first three decades shows an oscillating behavior. This is due to the different weights of the two terms appearing in Eq. (29) for each range of wavelengths. In particular, for  $k \lesssim 10^{-2} h \text{ Mpc}^{-1}$  the variance of  $\langle \delta \mathcal{F} \kappa \rangle$  is dominated by the first term, that is just the square of the signal. However, as the signal gets smaller with increasing  $k$ , for  $k \gtrsim 10^{-1} h \text{ Mpc}^{-1}$  it is the second term that dominates the variance.

Regarding  $\langle \delta \mathcal{F}^2 \kappa \rangle$ , it is necessary to point out two aspects. First, short wavelengths (high- $k$ ) modes provide the larger contribution to *both* the correlator *and* its standard deviation. Second, for  $k \gtrsim 10^{-2} h \text{ Mpc}^{-1}$  the ratio of the contribution to the correlator and to its standard deviation remain almost constant. This means that above  $10^{-2} h \text{ Mpc}^{-1}$  the different frequency ranges contribute roughly in the same proportion. This fact is both good news and bad news at the same time. It is bad news because it means that increasing the resolution of the Lyman- $\alpha$  spectra does not automatically translate into increasing the *precision* with which the correlator will be measured, as the high- $k$  modes that are introduced will boost both the correlator and its variance in the same way. On the other, this appears also to be good news because it tells us that low resolution spectra *which do not record non-linearities on small scales* can be successfully used to measure this correlation. To increase the S/N ratio and to achieve a better precision for this measurement it is better to increase the number of QSO spectra than to increase the resolution of each single spectra. Finally, cutting off the long-wavelength modes with  $k \lesssim 10^{-2} h \text{ Mpc}^{-1}$  should *not* have a great impact on the S/N ratio or on the measured value of the correlator: if on one hand the contribution of the modes with  $k \lesssim 10^{-2} h \text{ Mpc}^{-1}$  are noisier due to cosmic variance, on the other hand the absolute value of such contributions to the correlator and to its variance are negligible compared to the ones arising from  $k \gtrsim 10^{-2} h \text{ Mpc}^{-1}$ . We can see this fact also comparing the last column of Tab. IV with the right panel of Fig. 6 where the *absolute value* of the S/N ratio is plotted for varying values of the cutoffs  $k_L$  and  $k_C$ . By looking at the last column of Tab. IV we see that the ratio between the correlator and its standard deviation increases until about  $k \simeq 10^{-2} h \text{ Mpc}^{-1}$  where it

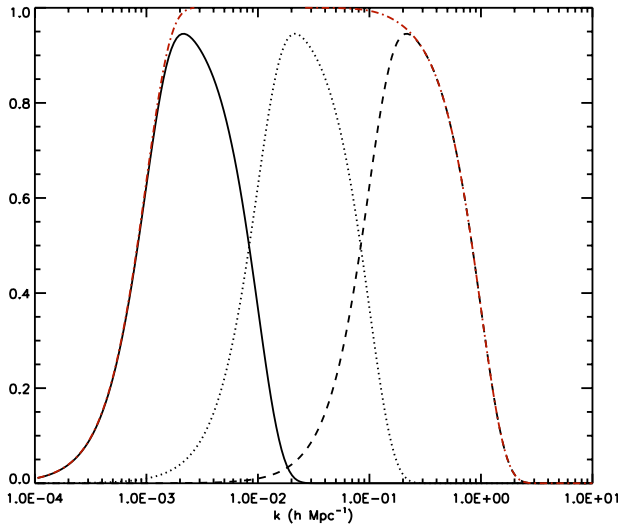


FIG. 5: Three filters used to calculate the contribution of the different modes to the correlators, their variance and the SN ratio. The filters have  $\{k_l = 10^{-3}, k_L = 10^{-2}\}$  (solid curve),  $\{k_l = 10^{-2}, k_L = 10^{-1}\}$  (dotted curve) and  $\{k_l = 10^{-1}, k_L = 1\}$  (dashed curve). Also shown is the sum of the filters (red dashed-dotted curve).



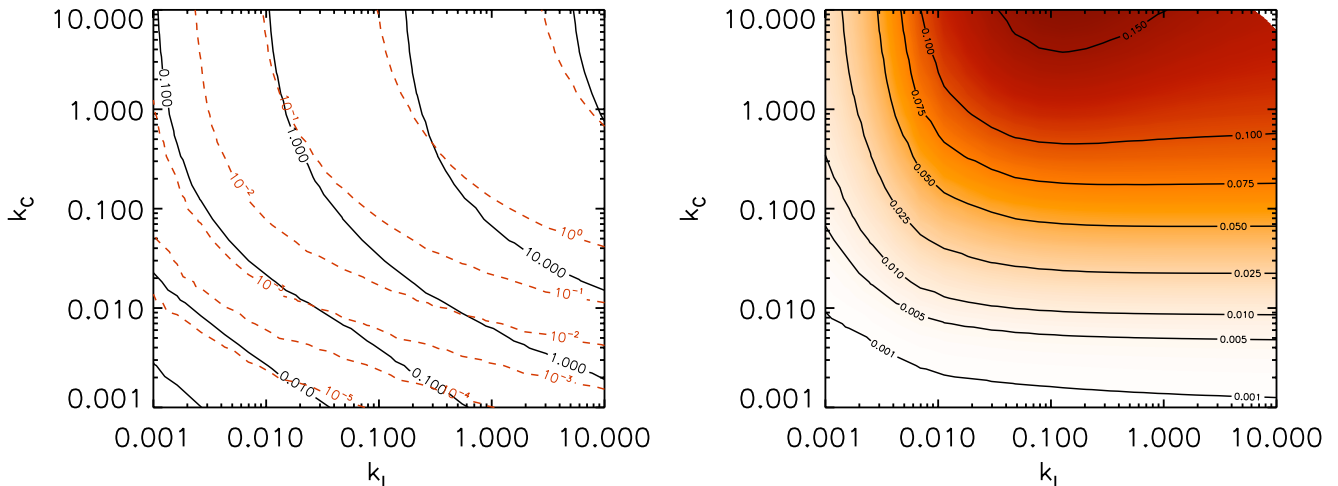


FIG. 6: Value of  $\langle \delta \mathcal{F}^2 \kappa \rangle$  (left panel, red dashed contours), of its standard deviation (left panel, black solid contour) and of its S/N ratio (right) for a single QSO lying at  $z = 2.6$  and whose spectrum covers  $\Delta z = 0.5$ . Here we assume  $k_l = 0$  and  $A = \beta = 1$ .

levels off. Looking at the right panel of Fig. 6 we notice exactly the same trend: increasing the resolution of the spectrum  $k_L$  above  $10^{-2} h \text{ Mpc}^{-1}$  does not improve the S/N ratio. This is because from that point on each new mode contributes in almost the same amount to the correlator *and to its standard deviation*.

#### Dependence on experimental resolutions

To analyze the impact of a change in the resolution of the experiments measuring the CMB convergence map or the Lyman- $\alpha$  flux we consider a single QSO at redshift  $z_0 = 2.6$  whose spectrum covers  $\Delta z = 0.5$  and vary  $k_L$  and  $k_C$ . In this case we set  $k_l = 0$ .

In Fig. 6 we show the value of  $\langle \delta \mathcal{F}^2 \kappa \rangle$ , of its standard deviation and of its S/N ratio for varying values of  $k_L$  and  $k_C$ . We note that both the correlator and its standard deviation increase with increasing resolution: this makes physical sense as increasing the resolution increases both the amount of information carried by each experiment and the cosmic variance associated with it. Except for very low values of  $k_C$ , an increase in the resolution of the Lyman- $\alpha$  spectrum is characterized by an almost equal amount of increase in both the correlator and its cosmic variance. This implies that the S/N becomes roughly constant for  $k_L \gtrsim 10^{-2} h \text{ Mpc}^{-1}$ . On the other hand, increasing  $k_C$  increases both the correlator and its cosmic variance only up to the point where  $k_C \simeq k_L$ .

### III. COSMOLOGICAL APPLICATIONS

#### A. Neutrinos

Massive neutrinos are known to suppress the growth of structure in the early universe on intermediate to small scales  $k \gtrsim 10^{-2} h \text{ Mpc}^{-1}$  [46]. Since  $\langle \delta \mathcal{F}^2 \kappa \rangle$  is mostly sensitive to the same range of scales, it seems reasonable to examine to what extent massive neutrinos will alter the  $\langle \delta \mathcal{F}^2 \kappa \rangle$  signal. The argument could also be turned around, asking how well a measurement of  $\langle \delta \mathcal{F}^2 \kappa \rangle$  would allow to constrain the sum of the neutrino masses. In this first work, we take the first route and we simply calculate how the  $\langle \delta \mathcal{F}^2 \kappa \rangle$  signal is affected by different values of the neutrino masses. We leave the analysis of the constraining power of  $\langle \delta \mathcal{F}^2 \kappa \rangle$  to a forthcoming work.

Quite generally massive neutrinos affect the matter density power spectrum in a scale dependent way (see [46] for a review). To account for this effect in an exact way it would require substantial modifications of the formalism and of the code that we are currently using to evaluate  $\langle \delta \mathcal{F}^2 \kappa \rangle$ . In particular, it would not be possible any longer to separate the integrations over the co-moving distance from the ones over the wavenumbers  $k$ . We leave this important development to a future project and for the purpose of this work we rely on the following approximation [47] for the growth of the dark matter perturbations

$$\delta_{\text{cdm}} \propto D(a)^{1-\frac{3}{5}f_\nu}, \quad (32)$$

where  $f_\nu \equiv \Omega_\nu / \Omega_m$ . The above expression should be accurate from the very large scales down to those mildly non-linear ones of the Lyman- $\alpha$  forest. Departures at

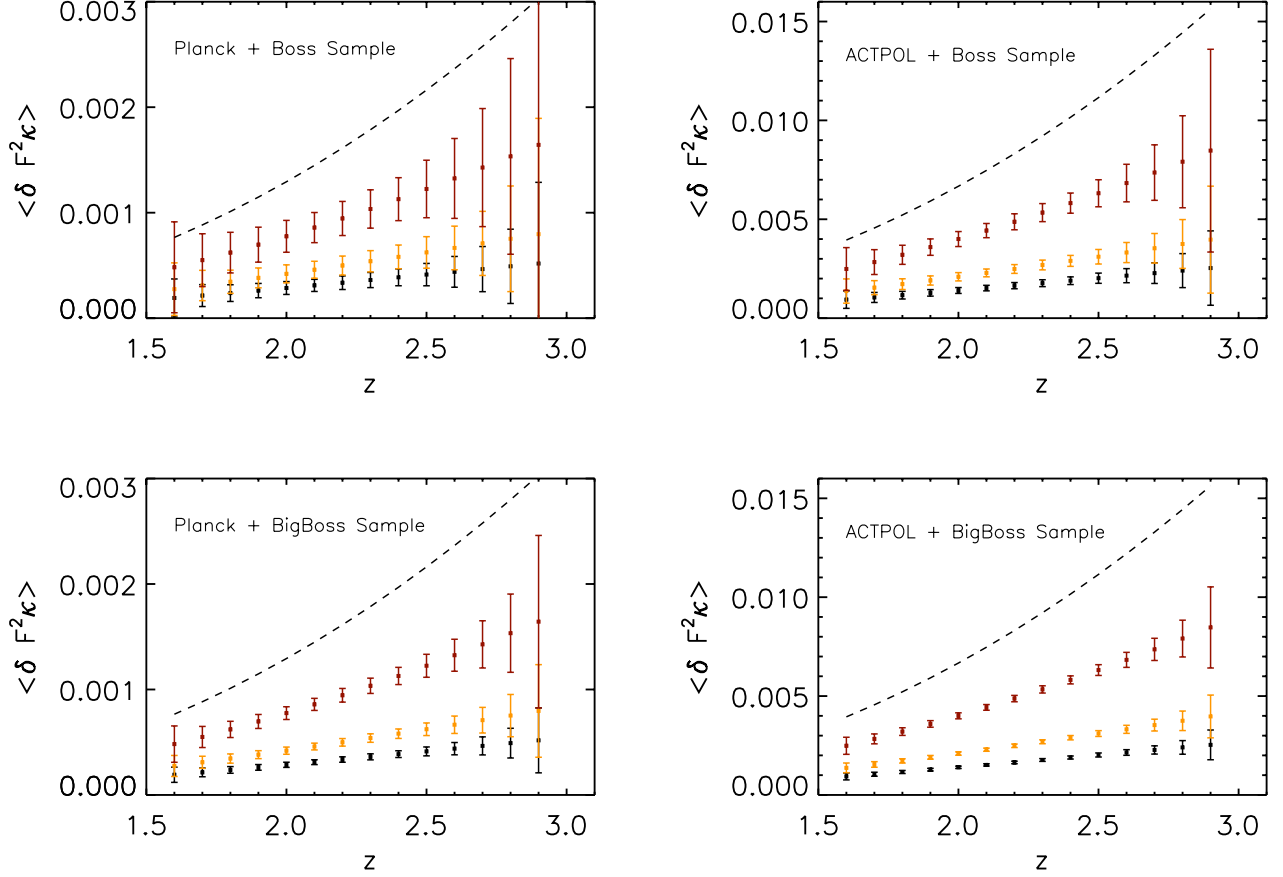


FIG. 7: Cross-correlation of the variance of the Lyman- $\alpha$  flux and CMB convergence as a function of redshift for the three different cosmological models with massive neutrinos shown in Table IV. Black, orange and red (with  $1\sigma$ ) error bars refer to  $\Sigma m_\nu(\text{eV}) = 0.54, 0.4, 0.15$ , respectively. The black dashed line shows the prediction for a massless neutrino cosmology consistent with WMAP-5 data. Four different cases are reported here for Planck+BOSS (top left), Planck + BigBOSS (bottom left), ACTPOL+BOSS (top right) and ACTPOL+BigBOSS (bottom right). The redshift evolution of  $A$  is here taken into account.

small scales are best handled with N-body or hydrodynamical codes [48].

The second aspect that we need to take into account before proceeding with the calculation is that consistency with CMB data requires that a change in the sum of the neutrino masses is accompanied by a change in the power spectrum normalization  $\sigma_8$  [12]. This fact has a profound consequence. Just by counting the number of powers of the power spectrum that enter in the different expressions, it is straightforward to note that  $\langle \delta \mathcal{F}^2 \kappa \rangle \sim \sigma_8^4$ , that  $\sigma_{\langle \delta \mathcal{F}^2 \kappa \rangle}^2 \sim \sigma_8^6$  and that its S/N ratio is proportional to  $\sigma_8$ . Consequently, a change in the neutrino masses, which requires a change in  $\sigma_8$  to maintain consistency with CMB data, will cause a change in  $\langle \delta \mathcal{F}^2 \kappa \rangle$ .

To take this into account we proceed as follows. First we consider the set of values allowed by the WMAP-5 data in the  $\sigma_8 - \Sigma m_\nu$  space at 95% CL. These correspond to the dark red area of the center panel of Fig. 17 in Komatsu et al. [12]. We then choose three flat mod-

Num.	$\Omega_m$	$\Omega_\Lambda$	$\Omega_\nu$	$\Sigma m_\nu(\text{eV})$	$\sigma_8$	h
1	0.269	0.719	1.2e-2	0.54	0.657	0.70
2	0.269	0.722	8.8e-3	0.40	0.708	0.70
3	0.269	0.728	3.3e-3	0.15	0.786	0.70
4	0.256	0.744	0.0	0.0	0.841	0.72

TABLE V: Values of the cosmological parameters assumed to estimate the effect of massive neutrinos on  $\langle \delta \mathcal{F}^2 \kappa \rangle$ . All models assume flat geometry.

els with massive neutrinos consistent with the WMAP-5 data and we use CAMB to generate the respective dark matter power spectra to be used in the calculation. The value of the cosmological parameters used for each model are summarized in Tab. V.

One last point is left to be considered. Note in fact that the S/N ratio for  $\langle \delta \mathcal{F}^2 \kappa \rangle$ , although increasing with

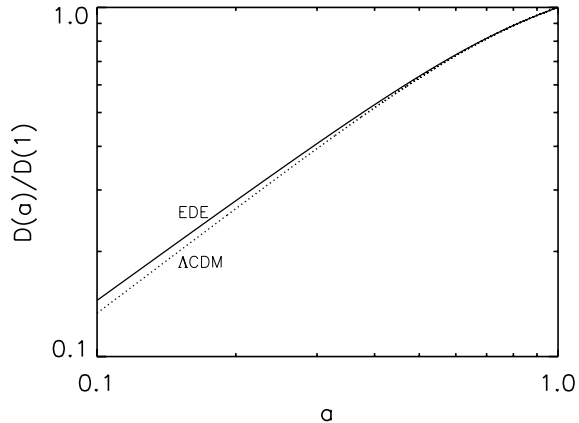


FIG. 8: Growth factors for the WMAP-5 flat  $\Lambda$ CDM cosmology (dotted curve) and for the early dark energy (EDE) model assumed in this section for comparison (solid curve).

$\Delta z$ , does not increase at a very high rate. It seems therefore possible to speculate that subdividing the Lyman- $\alpha$  spectra into sub-spectra, each of length  $dz = 0.1$ , despite lowering the S/N ratio for each single sub-spectrum, would allow to reach a better measurement of the redshift dependence of the signal.

Figure 7 below shows the result of applying the latter procedure. The black, orange and red data points represents predicted values of the  $\langle \delta \mathcal{F}^2 \kappa \rangle$  correlator for values of  $\sum m_\nu = \{0.54, 0.4, 0.15\}$  respectively, while the dashed black line shows the value of the correlator for a  $\Lambda$ CDM cosmology with massless neutrinos. As one can see, the cross-correlation signal is quite sensitive to the presence of massive neutrinos and already BOSS and Planck could provide constraints on the strength of such correlators. As pointed out above, this is due to the fact that more massive neutrinos requires smaller values of  $\sigma_8$ , which in turn depresses the signal.

It is here necessary to point out one important caveat. In this paper, we are making a tree-level approximation to the growth rate of  $k$  modes: this enables us to separate integrations along the comoving distances from integrations on the different modes. As previously mentioned, this approximation does not include the scale-dependent effects of neutrinos on the growth rate of structure. Similarly, this approximation also does not allow us to take into account the non-linearities induced by gravitational collapse, which on the other hand tend to enhance the power spectrum on small scales. We will need to either use Hyper-Extended Perturbation Theory results or non-linear simulations to evaluate these effects.

QSO sample	CMB Experiment	$\Delta\chi^2$
$1.6 \cdot 10^5$ (BOSS)	Planck	0.3451
$1.6 \cdot 10^5$ (BOSS)	ACTPOL	2.157
$1.0 \cdot 10^6$ (BigBOSS)	Planck	1.458
$1.0 \cdot 10^6$ (BigBOSS)	ACTPOL	9.117

TABLE VI: Summary of the estimated  $\Delta\chi^2$  between EDE and  $\Lambda$ CDM for four different combinations of future QSO and CMB experiments using the  $\langle \delta \mathcal{F}^2 \kappa \rangle$  correlator.

## B. Early Dark Energy

Since early dark energy or deviations from general relativity affect the growth rate of structure as a function of scale, the measurements of  $\langle \delta \mathcal{F}^2 \kappa \rangle(z)$  can in principle probe these effects. Here we focus on early dark energy (EDE) models, where dark energy makes a significant contribution to the energy density of the universe over a wide range of redshifts. The differences between EDE models and pure  $\Lambda$ CDM are particularly evident at high redshifts, when the former has been shown to influence the growth of the first cosmic structures both in the linear and in the non-linear regime.

We consider here the EDE model proposed in [49] and recently constrained by [50] (model EDE1 of [50]). We compare this model with the  $\Lambda$ CDM cosmology assumed until now. The differences in the growth factors for these two models is shown in Fig. 8 (the difference in the Hubble parameter evolution is smaller).

We quantify the departure of the correlators predicted for the EDE model from the  $\Lambda$ CDM one using the following expression:

$$\Delta\chi^2 = \sum_i \frac{(\langle \delta \mathcal{F}^n \kappa \rangle_{\text{EDE}} - \langle \delta \mathcal{F}^n \kappa \rangle_{\Lambda\text{CDM}})^2}{\sigma_{\text{EDE},i}^2}. \quad (33)$$

The results are shown in Fig. 9 and are summarized in Table IV. In this case the differences between EDE and  $\Lambda$ CDM are very limited and could only be appreciated at some significance with an advanced CMB experiment like ACTPOL and by increasing the number of spectroscopic QSOs with BigBOSS. However, it is worth stressing that the two models presented here are in perfect agreement with all the low redshift probes and the large-scale structure measurements provided by galaxy power spectra, CMB, Type Ia supernovae and Lyman- $\alpha$  forest. Therefore, possible departures from  $\Lambda$ CDM can be investigated only exploiting the capabilities of this intermediate redshift regime with such correlations or with similar observables in this redshift range.

## IV. CONCLUSIONS

This work presents a detailed investigation of the cross-correlation signals between transmitted Lyman- $\alpha$  flux

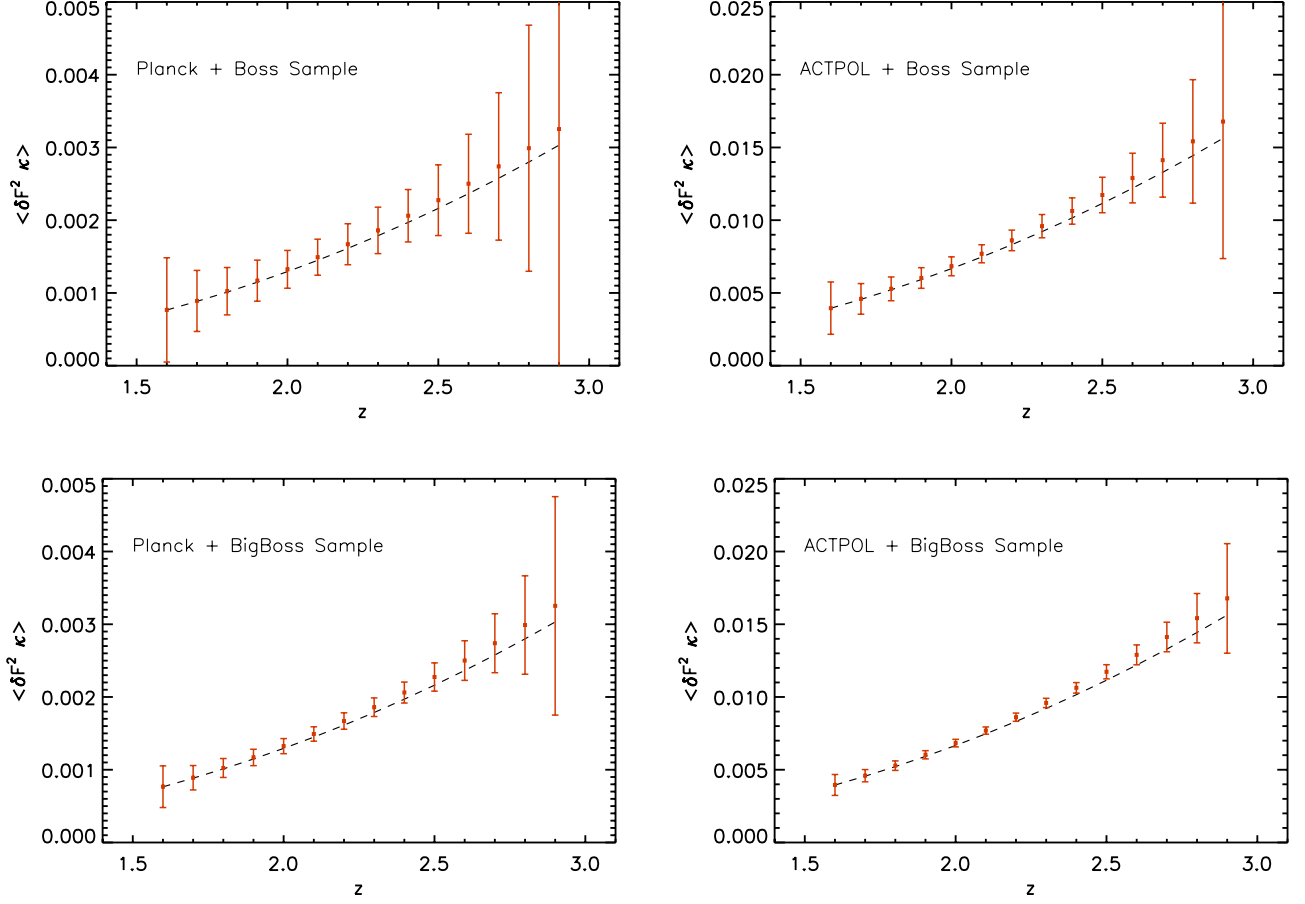


FIG. 9: Value of  $\langle \delta \mathcal{F}^2 \kappa \rangle$  estimated for the early dark energy EDE model of [49]. The dashed black line shows the expected value of the correlator for the  $\Lambda$ CDM cosmology assumed so far. Four different cases are reported here for Planck+BOSS (top left), Planck + BigBOSS (bottom left), ACTPOL+BOSS (top right) and ACTPOL+BigBOSS (bottom right). The redshift evolution of  $A$  is here taken into account.

and the weak lensing convergence of the CMB along the same line-of-sight. One of the motivations behind this work is that the Lyman- $\alpha$  forest has already been shown to be a powerful cosmological tool and novel ways of exploring and deepening the understanding of the flux/matter relation could significantly improve our knowledge of the high redshift universe. These correlators are able to provide astrophysical and cosmological information: since they are sensitive to both the flux/matter relation and the value of cosmological parameters, in principle they can be used to put constraints on both.

The correlators investigated in the present work have a clear physical meaning. The correlation of  $\delta \mathcal{F}$  with  $\kappa$  measures to what extent the fluctuations along the los mapped by the Lyman- $\alpha$  forest contribute to the CMB convergence field. This correlation is dominated by long wavelength modes ( $k \lesssim 10^{-1} h \text{ Mpc}^{-1}$ ) and as such is more sensitive to Lyman- $\alpha$  forest continuum fitting procedures. The correlation of the flux variance  $\delta \mathcal{F}^2$  with  $\kappa$

measures to what extent the growth of short wavelength modes (mapped by the Lyman- $\alpha$  flux) is enhanced or depressed by the fact that the latter are sitting in regions that are overdense or underdense on large scales. This interplay between short and long wavelength modes is well exemplified by the redshift dependence of the S/N ratio for  $\langle \delta \mathcal{F}^2 \kappa \rangle$ : lowering the redshift increases the S/N ratio because while the variance of  $\langle \delta \mathcal{F}^2 \kappa \rangle$  is dominated by the independent growth of long and short wavelength modes, the value of  $\langle \delta \mathcal{F}^2 \kappa \rangle$  itself receives an extra contribution due to the fact that the growth of the short wavelength modes is enhanced by the presence (and independent growth) of the long wavelength modes. Furthermore, this correlator is sensitive to intermediate-to-small scales ( $k \gtrsim 10^{-2} h \text{ Mpc}^{-1}$ ) and as such it should be less sensitive to Lyman- $\alpha$  forest continuum fitting procedures.

To estimate the values of the correlators, their variance and their S/N ratio we rely on linear theory and simple approximations, such as the fluctuating Gunn-Peterson



approximation at first order. Although the framework is simplified, the results are by no means obvious since different modes enter non-trivially in these quantities and in their signal-to-noise ratio. We estimate that such correlations may be detectable at a high significance level by Planck and the SDSS-III BOSS survey, experiments that are already collecting data. Moreover, our investigation of the modes of the Lyman- $\alpha$  forest that contribute to  $\langle \delta \mathcal{F}^2 \kappa \rangle$  shows that the low-resolution Lyman- $\alpha$  spectra measured by SDSS-III (which is aimed at the measurement of BAO at  $z = 2 - 4$  [37, 51]) should have enough resolution to yield a significant S/N.

The peculiar dependence of  $\langle \delta \mathcal{F}^2 \kappa \rangle$  on intermediate-to-short scales and its sensitivity to the value of the power spectrum normalization  $\sigma_8$  makes it a very useful cosmological tool to test all models characterized by variations of the power spectrum on such scales. In particular, we applied our estimates to evaluate the sensitivity of  $\langle \delta \mathcal{F}^2 \kappa \rangle$  to changes in  $\sigma_8$  due to variations in the sum of the neutrino masses and to show how promising this measurement could be in constraining the latter.

Finally, some caveats are in order. First, the code developed to estimate  $\langle \delta \mathcal{F}^2 \kappa \rangle$  and its variance is based on the tree-level perturbation theory results reported here. As such, the results shown do not take into account nonlinearities induced by gravitational collapse. The extension of the analytic results to take into account this aspect is actually quite straightforward, as it only requires the implementation of the so-called “HyperExtended Perturbation Theory” for the bispectrum [40]. However, the implementation of such changes in a numerical code are less trivial, as the integrations over the power spectrum and over the comoving distance cannot be factored any longer. We have nonetheless reason to speculate that the nonlinearities induced by gravitational collapse will not dramatically change the picture outlined here. At the redshift range spanned by the Lyman- $\alpha$  forest nonlinearities are normally mild and confined to short scales. Furthermore, as shown in Sec. II E, the S/N ratio for  $\langle \delta \mathcal{F}^2 \kappa \rangle$  dominated by modes with  $k \gtrsim 10^{-2} h \text{ Mpc}^{-1}$ , but all decades above  $10^{-2} h \text{ Mpc}^{-1}$  contribute in the same proportion to both the signal *and* its variance. It is therefore conceivable to filter out of the Lyman- $\alpha$  spectra the shortest scales, which are the most affected by nonlinearities and still be able to retain a non-negligible S/N.

The second caveat pertains the estimate of the correlators’ variance. It is in fact necessary to point out that to obtain such *estimates* Wick’s theorem has been applied. Whether the use of Wick’s theorem may or may not lead to an accurate result when considering the variance of  $\langle \delta \mathcal{F}^2 \kappa \rangle$  is debatable. On one hand it is possible to point out that the largest part of the signal arises at small separations, where the value of the correlator is dominated by its connected part. Analogously, it could be possi-

ble to argue that the use of Wick’s theorem may lead to underestimating the correlators’ variance. An exact evaluation of the variance of  $\langle \delta \mathcal{F}^2 \kappa \rangle$ , however, requires the exact calculation of a six point function, that to the best of our knowledge has never been determined. On the other hand it is also possible to point out that the connected part of  $\langle \delta_c \delta_{c'} \delta_q^2 \delta_{q'}^2 \rangle$  will be significantly non-zero only when the distances between the different points is small. As such, this term will give a non-zero contribution proportional to the length of the Lyman- $\alpha$  spectrum, which should be subdominant with respect to the ones considered in section II C, that are proportional to the distance from the observer all the way to the last scattering surface.

The third caveat pertains the expansion of the expression for the flux, Eq. (1). Despite the fact that the expansion carried out in Eq. (2) is correct on scales larger than about  $1 h^{-1} \text{ Mpc}$ , we point out here that the flux as expressed in Eq. (1) is intrinsically a non-linear function of the overdensity field. It is therefore reasonable to wonder whether the non-linearities induced by this non-linear mapping would somehow affect the conclusions presented here. A simple way to sidestep the present question is to undo the non-linear mapping by defining a new observable  $\hat{\mathcal{F}} = -\ln(\mathcal{F}) = A(1 + \delta_{\text{IGM}})^\beta$  and proceed by measuring its correlations.

The best way to assess to what extent the above caveats affect the estimates reported in the present work is through numerical simulations, calculating the convergence field on a light cone and at the same time measuring Lyman- $\alpha$  forest synthetic spectra and cross-correlating the two. This will be the next step in our investigation and the focus of the next publication.

Finally, on the analytical side we still need to address the estimate of the correlators when the power spectrum shows evolution in redshift *and* on different scales at the same time. As pointed out,  $\langle \delta \mathcal{F}^2 \kappa \rangle$  is sensitive to scales  $k \gtrsim 10^{-2} h \text{ Mpc}^{-1}$ . As such this correlator is an ideal tool to test modifications of gravity that show scale dependent growth. At the same time, this development would also allow the implementation of the hyperextended perturbation theory results and as such to address analytically the impact of gravity induced nonlinearities on the value of the correlators.

*Acknowledgements:* We thank S. Matarrese, F. Bernardeau, S. Dodelson, J. Frieman, E. Seftuss, N. Gnedin, R. Scoccimarro, S. Ho, D. Weinberg and J. P. Uzan for useful conversations. AV is supported by the DOE at Fermilab. MV is supported by grants PD51, ASI-AAE and a PRIN MIUR. DNS and SD are supported by NSF grant AST/0707731 and NASA theory grant NNX08AH30G. DNS thanks the APC (Paris) for its hospitality in spring 2008 when this project was initiated. AV thanks IAP (Paris) for hospitality during different stages of this project.

## APPENDIX A: DERIVATION OF PERTURBATIVE RESULTS FOR $\langle \delta \mathcal{F}^2 \kappa \rangle$

In this section we derive the expression for  $\langle \delta \mathcal{F}^2 \kappa \rangle$  shown in the text, Eqs. (19-21). We move from Eq. (5) and need to find an efficient way to evaluate  $\langle \delta^2(\hat{n}, \chi_q) \delta(\hat{n}, \chi_c) \rangle$ . We start by Fourier transforming this cumulant correlator to get

$$\begin{aligned}
\langle \delta_q^2 \delta_c \rangle &= \int \frac{d^3 \vec{k}_1}{(2\pi)^3} \frac{d^3 \vec{k}_2}{(2\pi)^3} \frac{d^3 \vec{k}_3}{(2\pi)^3} e^{i[(\vec{k}_1 + \vec{k}_2) \cdot \vec{x}_q + \vec{k}_3 \cdot \vec{x}_c]} W_\alpha(k_{1,\parallel}) W_\alpha(k_{2,\parallel}) W_\kappa(k_{3,\perp}) \langle \delta(\vec{k}_1) \delta(\vec{k}_2) \delta(\vec{k}_3) \rangle \\
&= \int \frac{d^3 \vec{k}_1}{(2\pi)^3} \frac{d^3 \vec{k}_2}{(2\pi)^3} \frac{d^3 \vec{k}_3}{(2\pi)^3} e^{i[(\vec{k}_1 + \vec{k}_2) \cdot \vec{x}_q + \vec{k}_3 \cdot \vec{x}_c]} (2\pi)^3 \delta_D^3(\vec{k}_1 + \vec{k}_2 + \vec{k}_3) W_\alpha(k_{1,\parallel}) W_\alpha(k_{2,\parallel}) W_\kappa(k_{3,\perp}) B(\vec{k}_1, \vec{k}_2, \vec{k}_3) \\
&= \int \frac{d^3 \vec{k}_1}{(2\pi)^3} \frac{d^3 \vec{k}_2}{(2\pi)^3} \frac{d^3 \vec{k}_3}{(2\pi)^3} e^{i[(\vec{k}_1 + \vec{k}_2) \cdot \vec{x}_q + \vec{k}_3 \cdot \vec{x}_c]} (2\pi)^3 \delta_D^3(\vec{k}_1 + \vec{k}_2 + \vec{k}_3) W_\alpha(k_{1,\parallel}) W_\alpha(k_{2,\parallel}) W_\kappa(k_{3,\perp}) \\
&\quad \times 2 \left[ F_2(\vec{k}_1, \vec{k}_2) P_L(\vec{k}_1, \chi_1) P_L(\vec{k}_2, \chi_2) + F_2(\vec{k}_2, \vec{k}_3) P_L(\vec{k}_2, \chi_2) P_L(\vec{k}_3, \chi_3) + F_2(\vec{k}_3, \vec{k}_1) P_L(\vec{k}_3, \chi_3) P_L(\vec{k}_1, \chi_1) \right].
\end{aligned} \tag{A1}$$

In the second line we introduced the bispectrum  $B(\vec{k}_1, \vec{k}_2, \vec{k}_3)$ , while in the third line we replaced the bispectrum with the expression for its kernel  $F_2$  and products of the linear matter power spectrum  $P_L(\vec{k}, \chi)$ . For sake of brevity, we keep implicit the dependence of the window functions on the cutoff scales:  $W_\alpha(k_{i,\parallel}) = W_\alpha(k_{i,\parallel}, k_L, k_t)$  and  $W_\kappa(k_{i,\perp}) = W_\kappa(k_{i,\perp}, k_C)$ . Next, we point out that the evaluation of Eq. (A1) requires in general the integration over a six dimensional  $k$ -space, which is further complicated by the fact that the different window functions break the spherical symmetry that one would normally exploit.

In what follows we adopt the tree level approximation to the bispectrum kernel,

$$F_2(\vec{k}_i, \vec{k}_j) = \frac{5}{7} + \frac{1}{2} \frac{\vec{k}_i \cdot \vec{k}_j}{k_i^2 k_j^2} (k_i^2 + k_j^2) + \frac{2}{7} \left( \frac{\vec{k}_i \cdot \vec{k}_j}{k_i k_j} \right)^2, \tag{A2}$$

which can readily be obtained from the more general expression derived by Scoccimarro and Couchman [40]

$$F_2^{HEPT}(\vec{k}_i, \vec{k}_j) = \frac{5}{7} a(n, k_i) a(n, k_j) + \frac{1}{2} \frac{\vec{k}_i \cdot \vec{k}_j}{k_i^2 k_j^2} (k_i^2 + k_j^2) b(n, k_i) b(n, k_j) + \frac{2}{7} \left( \frac{\vec{k}_i \cdot \vec{k}_j}{k_i k_j} \right)^2 c(n, k_i) c(n, k_j), \tag{A3}$$

setting the three auxiliary functions  $a(k)$ ,  $b(k)$  and  $c(k)$  that allow to account for non-linear growth of structure equal to unity. A generalization of the results shown below to take into account the more general formulation of Eq. (A3) is straightforward to derive.

To proceed further we note that each of the three terms appearing in the square bracket of Eq. (A1) depend only on *two* of the three wavevectors. When moving from the second to the third line, it is then essential *not* to carry out the integration over the delta function, because for *each* of these terms we integrate the Dirac  $\delta$  in order to obtain an expression that depends only on the same wavevectors that appear in the  $F_2$  kernel. The fact that two of the three physical points are the same also spoils the cyclic symmetry of the bispectrum. In particular, the  $\{1, 2\}$  term will differ from the  $\{2, 3\}$  and  $\{3, 1\}$  terms. We therefore let

$$\langle \delta_q^2 \delta_c \rangle = \langle \delta_q^2 \delta_c \rangle_{1,2} + 2 \langle \delta_q^2 \delta_c \rangle_{2,3}, \tag{A4}$$

and start by considering  $\langle \delta_q^2 \delta_c \rangle_{1,2}$ . Integrating over the  $\delta_D$  function in order to get rid of  $\vec{k}_3$  in favor of  $\vec{k}_1$  and  $\vec{k}_2$ , and then adopting a cylindrical coordinate system in  $k$ -space we get

$$\begin{aligned}
\langle \delta^2 \delta \rangle_{1,2} &= 2 \int \frac{dk_{1,\parallel}}{2\pi} \frac{dk_{2,\parallel}}{2\pi} e^{i(k_{1,\parallel} + k_{2,\parallel}) \Delta x} W_\alpha(k_{1,\parallel}) W_\alpha(k_{2,\parallel}) \int_{|k_{1,\parallel}|}^{\infty} \frac{k_1 dk_1}{(2\pi)^2} P(\vec{k}_1, \chi_1) \int_{|k_{2,\parallel}|}^{\infty} \frac{k_2 dk_2}{(2\pi)^2} P(\vec{k}_2, \chi_2) \\
&\quad \times \int d\phi \int d\theta_\perp F_2(\vec{k}_1, \vec{k}_2) W_\kappa[|\vec{k}_{1,\perp} + \vec{k}_{2,\perp}|].
\end{aligned} \tag{A5}$$

As also recognized in [52], the most challenging part of the calculation consists of the integration over the angular variables. This is because the convergence window function depends on  $|\vec{k}_{1,\perp} + \vec{k}_{2,\perp}|$ . The integration over the

angular variables in this case does not necessarily lead to an expression that may be numerically efficient to evaluate. In particular we aim to keep integrations factored as much as possible. Our first goal then is to integrate

$$\int d\phi \int d\theta_{\perp} F_2(\vec{k}_1, \vec{k}_2) W_{\kappa}[\vec{k}_{1,\perp} + \vec{k}_{2,\perp}] = 2\pi \exp\left(-\frac{k_{1,\perp}^2}{k_C^2}\right) \exp\left(-\frac{k_{2,\perp}^2}{k_C^2}\right) \times \int d\theta_{\perp} F_2(\vec{k}_1, \vec{k}_2) \exp\left[-2\frac{k_{1,\perp}k_{2,\perp}\cos(\theta_{\perp})}{k_C^2}\right], \quad (\text{A6})$$

where  $\theta_{\perp}$  is the angle between  $\vec{k}_{1,\perp}$  and  $\vec{k}_{2,\perp}$ . Now, as far as the integration over the angular variable is concerned, the kernel  $F_2$  can be written as

$$F_2(\vec{k}_1, \vec{k}_2) = R + S \cos(\theta_{\perp}) + T \cos^2(\theta_{\perp}), \quad (\text{A7})$$

where we have decomposed  $\vec{k}$  into its component parallel and perpendicular to the los according to  $\vec{k} = k_{\parallel}\hat{n} + \vec{k}_{\perp}$  and extracted the terms that are proportional to different powers of  $\cos(\theta_{\perp})$

$$R = \frac{5}{7} + \frac{1}{2} \frac{k_{1,\parallel} k_{2,\parallel}}{k_1^2 k_2^2} (k_1^2 + k_2^2) + \frac{2}{7} \left( \frac{k_{1,\parallel} k_{2,\parallel}}{k_1 k_2} \right)^2, \quad (\text{A8})$$

$$S = \frac{1}{2} \frac{k_{1,\perp} k_{2,\perp}}{k_1^2 k_2^2} (k_1^2 + k_2^2) + \frac{4}{7} \frac{k_{1,\parallel} k_{2,\parallel} k_{1,\perp} k_{2,\perp}}{k_1^2 k_2^2}, \quad (\text{A9})$$

$$T = \frac{2}{7} \left( \frac{k_{1,\perp} k_{2,\perp}}{k_1 k_2} \right)^2. \quad (\text{A10})$$

Integration over the angular variable can then be carried out by remembering that

$$\int_0^{2\pi} d\theta \exp[-\alpha \cos(\theta)] = 2\pi I_0(\alpha), \quad (\text{A11})$$

$$\int_0^{2\pi} d\theta \exp[-\alpha \cos(\theta)] \cos(\theta) = -2\pi I_1(\alpha), \quad (\text{A12})$$

$$\int_0^{2\pi} d\theta \exp[-\alpha \cos(\theta)] \cos^2(\theta) = \frac{2\pi}{\alpha} [I_1(\alpha) + \alpha I_2(\alpha)], \quad (\text{A13})$$

where  $I_n$  denotes the modified Bessel function of the first kind and n-th order. The integration over the angular variables yields

$$\int d\phi \int d\theta_{\perp} F_2(\vec{k}_1, \vec{k}_2) W_C[\vec{k}_{1,\perp} + \vec{k}_{2,\perp}] = (2\pi)^2 \exp\left(-\frac{k_{1,\perp}^2}{k_C^2}\right) \exp\left(-\frac{k_{2,\perp}^2}{k_C^2}\right) \times \left\{ R I_0\left(2\frac{k_{1,\perp}k_{2,\perp}}{k_C^2}\right) - S I_1\left(2\frac{k_{1,\perp}k_{2,\perp}}{k_C^2}\right) + T \left[ \frac{k_C^2}{2k_{1,\perp}k_{2,\perp}} I_1\left(2\frac{k_{1,\perp}k_{2,\perp}}{k_C^2}\right) + I_2\left(2\frac{k_{1,\perp}k_{2,\perp}}{k_C^2}\right) \right] \right\}.$$

The difficulty with this result is that every term depend on the product  $k_{1,\perp}k_{2,\perp}$ . As such, we are facing a 2D *joint* integration over the whole  $[k_{1,\perp}, k_{2,\perp}]$  domain. If on one hand this is doable, on the other hand we are more interested in obtaining a final result which is a product of integrals instead of the integral of the product. It is possible to move around this obstacle recalling that (Abramowitz and Stegun [53], 9.6.10)

$$I_{\nu}(z) = \sum_{n=0}^{\infty} \frac{1}{n! \Gamma(\nu + n + 1)} \left(\frac{z}{2}\right)^{2n+\nu} = \sum_{n=0}^{\infty} I_{\nu}^{(n)} \left(\frac{z}{2}\right)^{2n+\nu}. \quad (\text{A14})$$

We can write the modified Bessel function splitting the dependence on  $k_{1,\perp}$  and  $k_{2,\perp}$  as

$$I_0\left(2\frac{k_{1,\perp}k_{2,\perp}}{k_C^2}\right) = \sum_{n=0}^{\infty} I_0^{(n)} \left(\frac{k_{1,\perp}^2}{k_C^2}\right)^n \left(\frac{k_{2,\perp}^2}{k_C^2}\right)^n, \quad (\text{A15})$$

$$I_1\left(2\frac{k_{1,\perp}k_{2,\perp}}{k_C^2}\right) = \frac{k_{1,\perp}k_{2,\perp}}{k_C^2} \sum_{n=0}^{\infty} I_1^{(n)} \left(\frac{k_{1,\perp}^2}{k_C^2}\right)^n \left(\frac{k_{2,\perp}^2}{k_C^2}\right)^n, \quad (\text{A16})$$

$$I_2\left(2\frac{k_{1,\perp}k_{2,\perp}}{k_C^2}\right) = \left(\frac{k_{1,\perp}k_{2,\perp}}{k_C^2}\right)^2 \sum_{n=0}^{\infty} I_2^{(n)} \left(\frac{k_{1,\perp}^2}{k_C^2}\right)^n \left(\frac{k_{2,\perp}^2}{k_C^2}\right)^n, \quad (\text{A17})$$

where for sake of brevity we use the following notation for the coefficients

$$I_0^{(n)} = \frac{1}{n!^2}, \quad (\text{A18})$$

$$I_1^{(n)} = \frac{1}{n!(n+1)!} = \frac{I_0^{(n)}}{n+1}, \quad (\text{A19})$$

$$I_2^{(n)} = \frac{1}{n!(n+2)!} = \frac{I_0^{(n)}}{(n+1)(n+2)}. \quad (\text{A20})$$

Now, however complicated, this form allows us to factor the different integrals. Let's start by considering the term  $R I_0$ . We have

$$\begin{aligned} R I_0 &= \sum_{m=0}^{\infty} I_0^{(m)} \left( \frac{k_{1,\perp}^2}{k_C^2} \right)^m \left( \frac{k_{2,\perp}^2}{k_C^2} \right)^m \left[ \frac{5}{7} + \frac{1}{2} \frac{k_{1,\parallel} k_{2,\parallel}}{k_1^2 k_2^2} (k_1^2 + k_2^2) + \frac{2}{7} \left( \frac{k_{1,\parallel} k_{2,\parallel}}{k_1 k_2} \right)^2 \right] \\ &= \sum_{m=0}^{\infty} I_0^{(m)} \left( \frac{k_1^2 - k_{1,\parallel}^2}{k_C^2} \right)^m \left( \frac{k_2^2 - k_{2,\parallel}^2}{k_C^2} \right)^m \frac{5}{7} \\ &\quad + \sum_{m=0}^{\infty} I_0^{(m)} \left( \frac{k_1^2 - k_{1,\parallel}^2}{k_C^2} \right)^m \left( \frac{k_2^2 - k_{2,\parallel}^2}{k_C^2} \right)^m \left[ \frac{1}{2} \frac{k_{1,\parallel} k_{2,\parallel}}{k_1^2 k_2^2} (k_1^2 + k_2^2) \right] \\ &\quad + \sum_{m=0}^{\infty} I_0^{(m)} \left( \frac{k_1^2 - k_{1,\parallel}^2}{k_C^2} \right)^m \left( \frac{k_2^2 - k_{2,\parallel}^2}{k_C^2} \right)^m \left[ \frac{2}{7} \left( \frac{k_{1,\parallel} k_{2,\parallel}}{k_1 k_2} \right)^2 \right], \end{aligned} \quad (\text{A21})$$

where in going from the first to the second step we expressed  $k_{\perp}^2$  as a function of  $k$  and  $k_{\parallel}$  using the fact that  $k^2 = k_{\parallel}^2 + k_{\perp}^2$ . This is necessary because the power spectrum is function of  $k$  and not of  $k_{\perp}$ . We can then proceed by defining the following functions

$$\tilde{H}_m(k_{\parallel}, \chi; k_C) \equiv \int_{|k_{\parallel}|}^{\infty} \frac{k dk}{2\pi} \sqrt{I_0^{(m)}} P(k, \chi) \left( \frac{k^2 - k_{\parallel}^2}{k_C^2} \right)^m \exp \left( -\frac{k^2 - k_{\parallel}^2}{k_C^2} \right), \quad (\text{A22})$$

$$\tilde{L}_m(k_{\parallel}, \chi; k_C) \equiv \int_{|k_{\parallel}|}^{\infty} \frac{dk}{2\pi k} \sqrt{I_0^{(m)}} P(k, \chi) \left( \frac{k^2 - k_{\parallel}^2}{k_C^2} \right)^m \exp \left( -\frac{k^2 - k_{\parallel}^2}{k_C^2} \right). \quad (\text{A23})$$

It is important to notice that because of the integration domain *all* the above functions are *even* in  $k_{\parallel}$ , regardless of the value of  $m$ . With the help of these functions we then have

$$\begin{aligned} &\int_{|k_{1,\parallel}|}^{\infty} \frac{k_1 dk_1}{(2\pi)^2} P(\vec{k}_1, \chi_1) \int_{|k_{2,\parallel}|}^{\infty} \frac{k_2 dk_2}{(2\pi)^2} P(\vec{k}_2, \chi_2) \int d\phi \int d\theta_{\perp} R W_{\kappa}[|\vec{k}_{1,\perp} + \vec{k}_{2,\perp}|] \\ &= \frac{5}{7} \sum_{m=0}^{\infty} \tilde{H}_m(k_{1,\parallel}, \chi_1) \tilde{H}_m(k_{2,\parallel}, \chi_2) + \frac{2 k_{1,\parallel}^2 k_{2,\parallel}^2}{7} \sum_{m=0}^{\infty} \tilde{L}_m(k_{1,\parallel}, \chi_1) \tilde{L}_m(k_{2,\parallel}, \chi_2) \\ &\quad + \frac{k_{1,\parallel} k_{2,\parallel}}{2} \left[ \sum_{m=0}^{\infty} \tilde{H}_m(k_{1,\parallel}, \chi_1) \tilde{L}_m(k_{2,\parallel}, \chi_2) + \sum_{m=0}^{\infty} \tilde{L}_m(k_{1,\parallel}, \chi_1) \tilde{H}_m(k_{2,\parallel}, \chi_2) \right]. \end{aligned} \quad (\text{A24})$$

We have therefore succeeded in obtaining an expression that has the dependence on  $k_{1,\parallel}$  and  $k_{2,\parallel}$  *completely factored*. The sums over  $m$  and the fact that each term is a product of factors that only depend either on  $k_{1,\parallel}$  or on  $k_{2,\parallel}$  allows an integration term by term and at the same time to bypass the two dimensional joint integration.

We can then proceed exactly in the same way for the other two terms,  $S I_1$  and  $T I_2$  with the only difference that in order to obtain expressions where only the coefficients of the modified Bessel function of 0-th order  $I_0^{(m)}$  appear we use the fact that  $I_1^{(m)} = (m+1) I_0^{(m+1)}$ . We then obtain for the  $S$  term the following expression

$$\begin{aligned} &\int_{|k_{1,\parallel}|}^{\infty} \frac{k_1 dk_1}{(2\pi)^2} P(\vec{k}_1, \chi_1) \int_{|k_{2,\parallel}|}^{\infty} \frac{k_2 dk_2}{(2\pi)^2} P(\vec{k}_2, \chi_2) \int d\phi \int d\theta_{\perp} S \cos(\theta_{\perp}) W_{\kappa}[|\vec{k}_{1,\perp} + \vec{k}_{2,\perp}|] \\ &= -\frac{k_C^2}{2} \sum_{m=0}^{\infty} m \left[ \tilde{H}_m(k_{1,\parallel}, \chi_1) \tilde{L}_m(k_{2,\parallel}, \chi_2) + \tilde{L}_m(k_{1,\parallel}, \chi_1) \tilde{H}_m(k_{2,\parallel}, \chi_2) \right] - \frac{4 k_C^2 k_{1,\parallel} k_{2,\parallel}}{7} \sum_{m=0}^{\infty} m \tilde{L}_m(k_{1,\parallel}, \chi_1) \tilde{L}_m(k_{2,\parallel}, \chi_2). \end{aligned} \quad (\text{A25})$$



Finally, the  $T$  term gives

$$\begin{aligned} & \int_{|k_{1,\parallel}|}^{\infty} \frac{k_1 dk_1}{(2\pi)^2} P(\vec{k}_1, \chi_1) \int_{|k_{2,\parallel}|}^{\infty} \frac{k_2 dk_2}{(2\pi)^2} P(\vec{k}_2, \chi_2) \int d\phi \int d\theta_{\perp} T \cos^2(\theta_{\perp}) W_C[|\vec{k}_{1,\perp} + \vec{k}_{2,\perp}|] \\ &= \frac{k_C^4}{7} \sum_{m=0}^{\infty} m(2m-1) \tilde{L}_m(k_{1,\parallel}, \chi_1) \tilde{L}_m(k_{2,\parallel}, \chi_2). \end{aligned} \quad (\text{A26})$$

With the introduction of the definitions (A22-A23) and with the series expansion for the modified Bessel function we have therefore managed to carry out the integration over the perpendicular part of the wavevector. We are then left with the integration over  $k_{\parallel}$ . First recall that the window functions acting on the Lyman- $\alpha$  flux are

$$W_{\alpha}(k_{\parallel}, k_L, k_l) \equiv \left[ 1 - e^{-(k_{\parallel}/k_l)^2} \right] e^{-(k_{\parallel}/k_L)^2} = e^{-(k_{\parallel}/k_L)^2} - e^{-(k_{\parallel}/\bar{k})^2}, \quad (\text{A27})$$

and that in Eq. (A5) they decouple from one another. We can proceed further by defining the following function

$$f_m^{(n)}(\Delta\chi, \chi; k_C, k_L) \equiv \int_{-\infty}^{\infty} \frac{dk_{\parallel}}{2\pi} \left( \frac{k_{\parallel}}{k_L} \right)^n \exp \left[ -\frac{k_{\parallel}^2}{k_L^2} + ik_{\parallel} \Delta\chi \right] \tilde{f}_m(k_{\parallel}, \chi; k_C), \quad (\text{A28})$$

where  $f = \{H, L\}$ . It is straightforward to note that because all the tilde functions are even in  $k_{\parallel}$ , depending on the value of  $n$  the above Fourier transforms are either purely real (if  $n$  is even) or purely imaginary (if  $n$  is odd). Furthermore, if  $n$  is even the above functions are *real* and *even*, while if  $n$  is odd the above functions are *imaginary* and *odd*. Carrying out the integration on  $k_{\parallel}$  is then straightforward, as it just corresponds the replacement  $k_{\parallel}^n \tilde{f}_m(k_{\parallel}, \chi; k_C) \rightarrow k_L^n f_m^{(n)}(\Delta\chi, \chi; k_C, k_L) - \bar{k}^n f_m^{(n)}(\Delta\chi, \chi; k_C, \bar{k})$ . Finally, from a computational point of view this approach is rather efficient, as the tilded function need to be calculated only once and then used to construct the two-index functions.

With the help of these auxiliary functions we can finally obtain the following expression for the cumulant correlator  $\langle \delta^2 \delta \rangle_{1,2}$

$$\begin{aligned} \langle \delta^2 \delta \rangle_{1,2} &= 2 \sum_{m=0}^{\infty} \left\{ \frac{5}{7} \left[ H_m^{(0)}(\Delta\chi, \chi_q; k_C, k_L) - H_m^{(0)}(\Delta\chi, \chi_q; k_C, \bar{k}) \right]^2 \right. \\ &\quad + \left[ k_L H_m^{(1)}(\Delta\chi, \chi_q; k_C, k_L) - \bar{k} H_m^{(1)}(\Delta\chi, \chi_q; k_C, \bar{k}) \right] \left[ k_L L_m^{(1)}(\Delta\chi, \chi_q; k_C, k_L) - \bar{k} L_m^{(1)}(\Delta\chi, \chi_q; k_C, \bar{k}) \right] \\ &\quad - m k_C^2 \left[ H_m^{(0)}(\Delta\chi, \chi_q; k_C, k_L) - H_m^{(0)}(\Delta\chi, \chi_q; k_C, \bar{k}) \right] \left[ L_m^{(0)}(\Delta\chi, \chi_q; k_C, k_L) - L_m^{(0)}(\Delta\chi, \chi_q; k_C, \bar{k}) \right] \\ &\quad + \frac{2}{7} \left[ k_L^2 L_m^{(2)}(\Delta\chi, \chi_q; k_C, k_L) - \bar{k}^2 L_m^{(2)}(\Delta\chi, \chi_q; k_C, \bar{k}) \right]^2 \\ &\quad - \frac{4m}{7} k_C^2 \left[ k_L L_m^{(1)}(\Delta\chi, \chi_q; k_C, k_L) - \bar{k} L_m^{(1)}(\Delta\chi, \chi_q; k_C, \bar{k}) \right]^2 \\ &\quad \left. + \frac{m(2m-1)}{7} k_C^4 \left[ L_m^{(0)}(\Delta\chi, \chi_q; k_C, k_L) - L_m^{(0)}(\Delta\chi, \chi_q; k_C, \bar{k}) \right]^2 \right\}. \end{aligned} \quad (\text{A29})$$

A cautionary note is in order. As mentioned above, the functions defined through Eq. (A28) are purely imaginary if the index ( $n$ ) is odd. However, notice that in Eq. (A29) above there are always two such functions that appear together (as in the case with  $H_m^{(1)} L_m^{(1)}$ ), thus ensuring that  $\langle \delta^2 \delta \rangle_{1,2}$  is always real valued.

Let's now move to calculate  $\langle \delta^2 \delta \rangle_{2,3}$ . Notice incidentally that this term is exactly equal to  $\langle \delta^2 \delta \rangle_{3,1}$ . We start from the now usual expression

$$\begin{aligned} \langle \delta^2 \delta \rangle_{2,3} &= 2 \int \frac{dk_{2,\parallel}}{2\pi} \frac{dk_{3,\parallel}}{2\pi} e^{-i k_{3,\parallel} \Delta\chi} W_{\alpha}(-k_{2,\parallel} - k_{3,\parallel}) W_{\alpha}(k_{2,\parallel}) \int_{|k_{2,\parallel}|}^{\infty} \frac{k_2 dk_2}{(2\pi)^2} P(\vec{k}_2, \chi_2) \int_{|k_{3,\parallel}|}^{\infty} \frac{k_3 dk_3}{(2\pi)^2} P(\vec{k}_3, \chi_3) \\ &\quad \times \int d\phi \int d\theta_{\perp} F_2(\vec{k}_2, \vec{k}_3) W_{\kappa}(\vec{k}_{3,\perp}), \end{aligned} \quad (\text{A30})$$

where, as previously, we have traded the integrations over  $k_{i,\perp}$  for the ones over  $k_i$ . In this case the integration over the angular variables doesn't pose any problem as the window function  $W_{\kappa}$  is actually a function of  $k_{3,\perp}$  only and it can be safely pulled out of the angular integrals

$$\int d\phi \int d\theta_{\perp} F_2(\vec{k}_2, \vec{k}_3) = \frac{(2\pi)^2}{7} (5+1) + \frac{(2\pi)^2}{2} k_{2,\parallel} k_{3,\parallel} \left( \frac{1}{k_2^2} + \frac{1}{k_3^2} \right) + \frac{(2\pi)^2}{7} \left[ 3 \frac{k_{2,\parallel}^2 k_{3,\parallel}^2}{k_2^2 k_3^2} - \left( \frac{k_{2,\parallel}^2}{k_2^2} + \frac{k_{3,\parallel}^2}{k_3^2} \right) \right] \quad (\text{A31})$$

It is here necessary to point out that since  $W_\kappa$  depends only on  $k_{3,\perp}$ , the tilded functions that will appear when the integration over  $k_2$  is carried out will contain no filter function. We characterize these functions by substituting to  $k_C$  the  $\infty$  symbol, as to all extent the gaussian filter with  $k_C \rightarrow \infty$  just yields unity. We then have

$$\begin{aligned}
& \int_{|k_{2,\parallel}|}^{\infty} \frac{k_2 dk_2}{(2\pi)^2} P(\vec{k}_2, \chi_2) \int_{|k_{3,\parallel}|}^{\infty} \frac{k_3 dk_3}{(2\pi)^2} P(\vec{k}_3, \chi_3) \int d\phi \int d\theta_{\perp} F_2(\vec{k}_2, \vec{k}_3) W_\kappa(\vec{k}_{3,\perp}) \\
&= \int_{|k_{2,\parallel}|}^{\infty} \frac{k_2 dk_2}{(2\pi)^2} P(\vec{k}_2, \chi_2) \int_{|k_{3,\parallel}|}^{\infty} \frac{k_3 dk_3}{(2\pi)^2} P(\vec{k}_3, \chi_3) \exp\left(-\frac{k_3^2 - k_{3,\parallel}^2}{k_C^2}\right) \\
&\times (2\pi)^2 \left[ \frac{5}{7} + \frac{1}{2} k_{2,\parallel} k_{3,\parallel} \left( \frac{1}{k_2^2} + \frac{1}{k_3^2} \right) + \frac{1}{7} \frac{1}{k_2^2 k_3^2} (2 k_{2,\parallel}^2 k_{3,\parallel}^2 + k_{2,\perp}^2 k_{3,\perp}^2) \right] \\
&= \frac{6}{7} \tilde{H}_0(k_{2,\parallel}, \chi_2; \infty) \tilde{H}_0(k_{3,\parallel}, \chi_3; k_C) + \frac{1}{2} k_{2,\parallel} k_{3,\parallel} \tilde{L}_0(k_{2,\parallel}, \chi_2; \infty) \tilde{H}_0(k_{3,\parallel}, \chi_3; k_C) \\
&+ \frac{1}{2} k_{2,\parallel} k_{3,\parallel} \tilde{H}_0(k_{2,\parallel}, \chi_2; \infty) \tilde{L}_0(k_{3,\parallel}, \chi_3; k_C) + \frac{3}{7} k_{2,\parallel}^2 k_{3,\parallel}^2 \tilde{L}_0(k_{2,\parallel}, \chi_2; \infty) \tilde{L}_0(k_{3,\parallel}, \chi_3; k_C) \\
&- \frac{1}{7} k_{3,\parallel}^2 \tilde{H}_0(k_{2,\parallel}, \chi_2; \infty) \tilde{L}_0(k_{3,\parallel}, \chi_3; k_C) - \frac{1}{7} k_{2,\parallel}^2 \tilde{L}_0(k_{2,\parallel}, \chi_2; \infty) \tilde{H}_0(k_{3,\parallel}, \chi_3; k_C). \tag{A32}
\end{aligned}$$

The expression for the window function acting on the Lyman- $\alpha$  flux is in this case

$$\begin{aligned}
W_\alpha(-k_{2,\parallel} - k_{3,\parallel}) W_\alpha(k_{2,\parallel}) &= \left[ 1 - e^{-\left(\frac{k_{2,\parallel} + k_{3,\parallel}}{k_L}\right)^2} \right] e^{-\left(\frac{k_{2,\parallel} + k_{3,\parallel}}{k_L}\right)^2} \left[ 1 - e^{-\left(\frac{k_{2,\parallel}}{k_L}\right)^2} \right] e^{-\left(\frac{k_{2,\parallel}}{k_L}\right)^2} \\
&= e^{-k_{3,\parallel}^2/k_L^2} \left( e^{-2k_{2,\parallel}^2/k_L^2} - e^{-k_{2,\parallel}^2/\hat{k}^2} \right) \sum_n \frac{(-2)^n}{n!} \left( \frac{k_{2,\parallel}}{k_L} \right)^n \left( \frac{k_{3,\parallel}}{k_L} \right)^n \\
&+ e^{-k_{3,\parallel}^2/\bar{k}^2} \left( e^{-2k_{2,\parallel}^2/\bar{k}^2} - e^{-k_{2,\parallel}^2/\hat{k}^2} \right) \sum_n \frac{(-2)^n}{n!} \left( \frac{k_{2,\parallel}}{\bar{k}} \right)^n \left( \frac{k_{3,\parallel}}{\bar{k}} \right)^n, \tag{A33}
\end{aligned}$$

where we have recast the window function in a combination that is suitable for furthering the calculation. Notice in fact that the first and second term in the sum differ only by the presence of  $k_L$  or  $\bar{k}$  in the denominators of the exponentials. Furthermore, the terms in square brackets are functions of  $k_{2,\parallel}$  only. We then define the coefficients

$$\bar{f}_m^{(n)}(\chi; k_L) \equiv \int_{-\infty}^{\infty} \frac{dk_{\parallel}}{2\pi} \left( \frac{k_{\parallel}}{k_L} \right)^n \left[ e^{-2k_{\parallel}^2/k_L^2} - e^{-k_{\parallel}^2/\hat{k}^2} \right] \tilde{f}_m(k_{\parallel}, \chi, \infty), \tag{A34}$$

$$\bar{f}_m^{(n)}(\chi; \bar{k}) \equiv \int_{-\infty}^{\infty} \frac{dk_{\parallel}}{2\pi} \left( \frac{k_{\parallel}}{\bar{k}} \right)^n \left[ e^{-2k_{\parallel}^2/\bar{k}^2} - e^{-k_{\parallel}^2/\hat{k}^2} \right] \tilde{f}_m(k_{\parallel}, \chi, \infty). \tag{A35}$$

A point worth making is that the second expression can be obtained from the first one with the substitution  $k_L \rightarrow \bar{k}$  in the denominators but *not* in the expression for  $\hat{k}$ , hence the necessity of two separate definitions. Considering then the following generic term, it is possible to show that

$$\begin{aligned}
& \int \frac{dk_2}{2\pi} \frac{dk_3}{2\pi} k_2^p k_3^q \tilde{f}_i(k_2, \chi_2; \infty) \tilde{g}_j(k_3, \chi_3; k_C) W_\alpha(-k_2 - k_3) W_\alpha(k_2) e^{-ik_3 \Delta\chi} \\
&= \sum_m \frac{(-2)^m}{m!} \left[ k_L^{(p+q)} g_j^{(q+m)}(\Delta\chi, \chi; k_C, k_L) \bar{f}_i^{(p+m)}(\chi_2, k_L) + \bar{k}^{(p+q)} g_j^{(q+m)}(\Delta\chi, \chi; k_C, \bar{k}) \bar{f}_i^{(p+m)}(\chi_2, \bar{k}) \right], \tag{A36}
\end{aligned}$$

which then leads directly to

$$\begin{aligned}
\langle \delta_q^2 \delta_c \rangle_{2,3} &= 2 \sum_{m=0}^{\infty} \frac{(-1)^m 2^m}{m!} \left[ \frac{6}{7} \bar{H}_0^{(m)}(k_L) H_0^{(m)}(\Delta\chi; k_C, k_L) + \frac{1}{2} k_L^2 \bar{L}_0^{(m+1)}(k_L) H_0^{(m+1)}(\Delta\chi; k_C, k_L) \right. \\
&+ \frac{1}{2} k_L^2 \bar{H}_0^{(m+1)}(k_L) L_0^{(m+1)}(\Delta\chi; k_C, k_L) + \frac{3}{7} k_L^4 \bar{L}_0^{(m+2)}(k_L) L_0^{(m+2)}(\Delta\chi; k_C, k_L) \\
&- \left. \frac{k_L^2}{7} \bar{H}_0^{(m)}(k_L) L_0^{(m+2)}(\Delta\chi; k_C, k_L) - \frac{k_L^2}{7} \bar{L}_0^{(m+2)}(k_L) H_0^{(m)}(\Delta\chi; k_C, k_L) + (k_L \rightarrow \bar{k}) \right]. \tag{A37}
\end{aligned}$$

Note that in the above expression while  $\bar{f}_m^{(n)}$  are always real, the  $f_m^{(n)}$  can be real or imaginary depending on whether  $n$  is even or odd. However, the fact that  $\bar{f}_m^{(n)}$  is zero whenever the upper index is odd guarantees that  $\langle \delta^2 \delta \rangle_{2,3}$  is always

real valued. Also, notice that while the coefficients  $\bar{f}_m^{(n)}(\chi_Q; k_L)$  are decreasing with  $m$ , the coefficients  $\bar{f}_m^{(n)}(\chi_Q; \bar{k})$  are actually *increasing* with  $m$ . However, the  $m!$  factor present in the denominator more than compensates for these increasing coefficients and allows to truncate the series in an actual calculation.

Finally, it is worth pointing out that the case without cutoff on the long wavelength mode is recovered from the above expression simply by setting  $k_l = 0$  and then noticing that in this case  $\bar{k} = 0$  and that therefore the corresponding terms appearing in Eqs. (A29, A37) disappear.

- 
- [1] <http://www.rssd.esa.int/index.php?project=planck>.
- [2] <http://www.physics.princeton.edu/act>.
- [3] A. D. Hincks, V. Acquaviva, P. Ade, P. Aguirre, M. Amiri, J. W. Appel, L. F. Barrientos, E. S. Battistelli, J. R. Bond, B. Brown, et al., ArXiv e-prints (2009), 0907.0461.
- [4] <http://pole.uchicago.edu>.
- [5] Z. Staniszewski, P. A. R. Ade, K. A. Aird, B. A. Benson, L. E. Bleem, J. E. Carlstrom, C. L. Chang, H. Cho, T. M. Crawford, A. T. Crites, et al., ApJ **701**, 32 (2009), 0810.1578.
- [6] The QU Imaging Experiment <http://quiet.uchicago.edu/>.
- [7] <http://bolo.berkeley.edu/polarbear/>.
- [8] P. McDonald, U. Seljak, R. Cen, D. Shih, D. H. Weinberg, S. Burles, D. P. Schneider, D. J. Schlegel, N. A. Bahcall, J. W. Briggs, et al., ApJ **635**, 761 (2005), arXiv:astro-ph/0407377.
- [9] U. Seljak, A. Makarov, P. McDonald, S. F. Anderson, N. A. Bahcall, J. Brinkmann, S. Burles, R. Cen, M. Doi, J. E. Gunn, et al., Phys. Rev. D **71**, 103515 (2005), arXiv:astro-ph/0407372.
- [10] D. J. Schlegel et al. (2009), 0904.0468.
- [11] A. Lewis and A. Challinor, Phys. Rep. **429**, 1 (2006), arXiv:astro-ph/0601594.
- [12] E. Komatsu et al. (WMAP), Astrophys. J. Suppl. **180**, 330 (2009), 0803.0547.
- [13] W. Hu and T. Okamoto, ApJ **574**, 566 (2002), arXiv:astro-ph/0111606.
- [14] C. M. Hirata and U. Seljak, Phys. Rev. D **68**, 083002 (2003), arXiv:astro-ph/0306354.
- [15] J. Yoo and M. Zaldarriaga, ArXiv e-prints **805** (2008), 0805.2155.
- [16] H. V. Peiris and D. N. Spergel, ApJ **540**, 605 (2000), arXiv:astro-ph/0001393.
- [17] T. Giannantonio, R. Scranton, R. G. Crittenden, R. C. Nichol, S. P. Boughn, A. D. Myers, and G. T. Richards, Phys. Rev. D **77**, 123520 (2008), 0801.4380.
- [18] C. M. Hirata, S. Ho, N. Padmanabhan, U. Seljak, and N. A. Bahcall, Phys. Rev. D **78**, 043520 (2008), 0801.0644.
- [19] R. A. C. Croft, A. J. Banday, and L. Hernquist, MNRAS **369**, 1090 (2006), arXiv:astro-ph/0512380.
- [20] J.-Q. Xia, M. Viel, C. Baccigalupi, and S. Matarrese, JCAP **0909**, 003 (2009), 0907.4753.
- [21] J. E. Gunn and B. A. Peterson, Astrophys. J. **142**, 1633 (1965).
- [22] T.-S. Kim, J. S. Bolton, M. Viel, M. G. Haehnelt, and R. F. Carswell, MNRAS **382**, 1657 (2007), 0711.1862.
- [23] L. Hui and N. Y. Gnedin, Mon. Not. Roy. Astron. Soc. **292**, 27 (1997), astro-ph/9612232.
- [24] P. McDonald, ApJ **585**, 34 (2003), arXiv:astro-ph/0108064.
- [25] M. McQuinn, A. Lidz, M. Zaldarriaga, L. Hernquist, P. F. Hopkins, S. Dutta, and C.-A. Faucher-Giguère, ApJ **694**, 842 (2009), 0807.2799.
- [26] H. Bi and A. F. Davidsen, Astrophys. J. **479**, 523 (1997), astro-ph/9611062.
- [27] R. A. C. Croft, D. H. Weinberg, N. Katz, and L. Hernquist, ApJ **495**, 44 (1998), arXiv:astro-ph/9708018.
- [28] R. A. C. Croft, D. H. Weinberg, M. Bolte, S. Burles, L. Hernquist, N. Katz, D. Kirkman, and D. Tytler, ApJ **581**, 20 (2002), arXiv:astro-ph/0012324.
- [29] M. Viel, S. Matarrese, H. J. Mo, M. G. Haehnelt, and T. Theuns, Mon. Not. Roy. Astron. Soc. **329**, 848 (2002), astro-ph/0105233.
- [30] F. Saitta, V. D'Odorico, M. Bruscoli, S. Cristiani, P. Monaco, and M. Viel, MNRAS **385**, 519 (2008), 0712.2452.
- [31] D. J. Eisenstein and W. Hu, ApJ **496**, 605 (1998), arXiv:astro-ph/9709112.
- [32] S. Zaroubi, M. Viel, A. Nusser, M. Haehnelt, and T.-S. Kim, MNRAS **369**, 734 (2006), arXiv:astro-ph/0509563.
- [33] N. Y. Gnedin and L. Hui, MNRAS **296**, 44 (1998), arXiv:astro-ph/9706219.
- [34] M. Viel, M. G. Haehnelt, and V. Springel, MNRAS **367**, 1655 (2006), arXiv:astro-ph/0504641.
- [35] T. Fang and M. White, AstroPhysical Journal Letters **606**, L9 (2004), arXiv:astro-ph/0312280.
- [36] R. A. C. Croft, ApJ **610**, 642 (2004), arXiv:astro-ph/0310890.
- [37] A. Slosar, S. Ho, M. White, and T. Louis, ArXiv e-prints (2009), 0906.2414.
- [38] A. Vallinotto, S. Das, D. N. Spergel, and M. Viel, Physical Review Letters **103**, 091304 (2009), 0903.4171.
- [39] M. Zaldarriaga, U. Seljak, and L. Hui, ApJ **551**, 48 (2001), arXiv:astro-ph/0007101.
- [40] R. Scoccimarro and H. M. P. Couchman, Mon. Not. Roy. Astron. Soc. **325**, 1312 (2001), astro-ph/0009427.
- [41] W. Hu and T. Okamoto, Astrophys. J. **574**, 566 (2002), astro-ph/0111606.
- [42] V. AA. (Planck) (2006), astro-ph/0604069.
- [43] M. Viel, S. Matarrese, A. Heavens, M. G. Haehnelt, T.-S. Kim, V. Springel, and L. Hernquist, MNRAS **347**, L26 (2004), arXiv:astro-ph/0308151.
- [44] U. Seljak, P. McDonald, and A. Makarov, MNRAS **342**, L79 (2003), arXiv:astro-ph/0302571.
- [45] D. Schlegel, M. White, and D. Eisenstein, ArXiv e-prints (2009), 0902.4680.
- [46] J. Lesgourgues and S. Pastor, Phys. Rept. **429**, 307 (2006), astro-ph/0603494.
- [47] W. Hu and D. J. Eisenstein, Astrophys. J. **498**, 497 (1998), astro-ph/9710216.
- [48] J. Brandbyge, S. Hannestad, T. Haugbølle, and B. Thomsen, Journal of Cosmology and Astro-Particle Physics **8**,

- 20 (2008), 0802.3700.
- [49] E. V. Linder, *Astroparticle Physics* **26**, 16 (2006), arXiv:astro-ph/0603584.
  - [50] J.-Q. Xia and M. Viel, *JCAP* **0904**, 002 (2009), 0901.0605.
  - [51] P. McDonald and D. J. Eisenstein, *Phys. Rev. D* **76**, 063009 (2007), arXiv:astro-ph/0607122.
  - [52] F. Bernardeau, *Astron. Astrophys.* **312**, 11 (1996), astro-ph/9602072.
  - [53] M. Abramowitz and I. A. Stegun, *Handbook of mathematical functions: with formulas, graphs, and mathematical tables* (Dover Publications, New York, 1965).